University of Thessaly
School of Engineering
Department of Mechanical Engineering

3-DIMENSIONAL THERMAL ANALYSIS OF ADDITIVE MANUFACTURING PROCESSES

by

KONSTANTINOS GALENOS

Submitted in partial fulfillment of the requirements for the degree of Diploma in Mechanical Engineering at the University of Thessaly

Volos,2023

University of Thessaly
School of Engineering
Department of Mechanical Engineering

3-DIMENSIONAL THERMAL ANALYSIS OF ADDITIVE MANUFACTURING PROCESSES

by

KONSTANTINOS GALENOS

Submitted in partial fulfillment of the requirements for the degree of Diploma in Mechanical Engineering at the University of Thessaly

Volos,2023

Approved by the Committee on Final Examination:

Advisor — *Dr. Nikolaos Aravas*
Professor of Computational Mechanics,
Department of Mechanical Engineering, University of Thessaly

Member — *Dr. Gregory Haidemenopoulos*
Professor of Physical Mettalurgy,
Department of Mechanical Engineering, University of Thessaly

Member — *Dr. Emmanouil Bouzakis*
Associate Professor of Manufacturing Processes,
Department of Mechanical Engineering, University of Thessaly

3-DIMENSIONAL THERMAL ANALYSIS OF ADDITIVE MANUFACTURING PROCESSES

GALENOS KONSTANTINOS
Department of Mechanical Engineering, University of Thessaly

Supervisor : Dr. Nikolaos Aravas
Professor of Computational Mechanics

Abstract

Additive Manufacturing (AM) has seen significant growth and widespread adoption in various industries in recent years, with laser-based AM being one of the most promising technologies for producing complex metal parts. However, the quality of the parts produced by laser-based AM is impacted by the resulting microstructure, residual stresses, and distortion, which are in turn affected by the thermal history produced during the process. To address this issue, this diploma thesis presents a three-dimensional model that numerically determines the temperature distribution of laser-based AM processes using metal powder, applicable to various process conditions. The thermal behavior of the system, including the repeated high-energy heat source thermal cycles, the melting and solidification of metal powder in the molten pool, and the application of appropriate convective and radiant boundary conditions at each free surface during element activation, is modeled and simulated using the Finite Element Method (FEM). The FEM software ABAQUS is used to simulate the thermal behavior of a three-dimensional laser-based AM process for metallic parts and calculate the temperature field. The three-dimensional model developed in this thesis enables a better understanding of the thermal behavior of the laser-based AM process and computes the temperature field for various process conditions. These data can be used in future studies to estimate residual stresses and distortion, as well as to evaluate the resulting microstructure.

Contents

List of Tables

List of Figures

Chapter 1

Introduction

Additive manufacturing (AM) enables direct fabrication of a model created through a three-dimensional Computer-Aided Design (3D CAD) system, eliminating the requirement for process planning. Parts are manufactured by depositing material or by joining it together in layers, where each layer is a thin cross-section of the part derived from the original CAD data. Unlike traditional manufacturing methods that often involve removing material through techniques such as milling, machining, carving, or shaping, additive manufacturing leads to a significant reduction in material waste and lower costs, as well as shorter production times. Initially, AM was used specifically to create visualization models during product development (rapid prototyping), however these technologies have advanced to the point that the product is suitable for end-use. Additive manufacturing was originally developed around polymeric materials, but as the technology progressed the application range extended even further, to include the direct production of metallic parts through the use of high-powered laser technologies [1].
Laser-based AM has seen significant growth and widespread adoption across various industries, including tool-making, aerospace, and biomedical, in recent years [2, 3]. There are two types of AM in which a high-power heat source is utilized to create a molten pool of metal powder which then solidifies to form a fully dense layer :

1. Directed Energy Deposition (DED) (Figure 1.1a) is a process of adding material to a substrate using a concentrated beam of energy such as a laser or an electron beam. In metal powder directed energy deposition, a stream of metal powder is fed into the focus of the energy beam, where it is melted and deposited onto the substrate to build up the desired three-dimensional shape.

2. Powder Bed Fusion (PBF) (Figure 1.1b) is a type of AM process in which a part is built up layer by layer from a bed of metal powder. The process works by spreading a thin layer of metal powder over the build area and then selectively fusing the powder particles together using a concentrated heat source, such as a laser or an electron beam. The process is repeated for each successive layer until the desired part geometry is achieved.

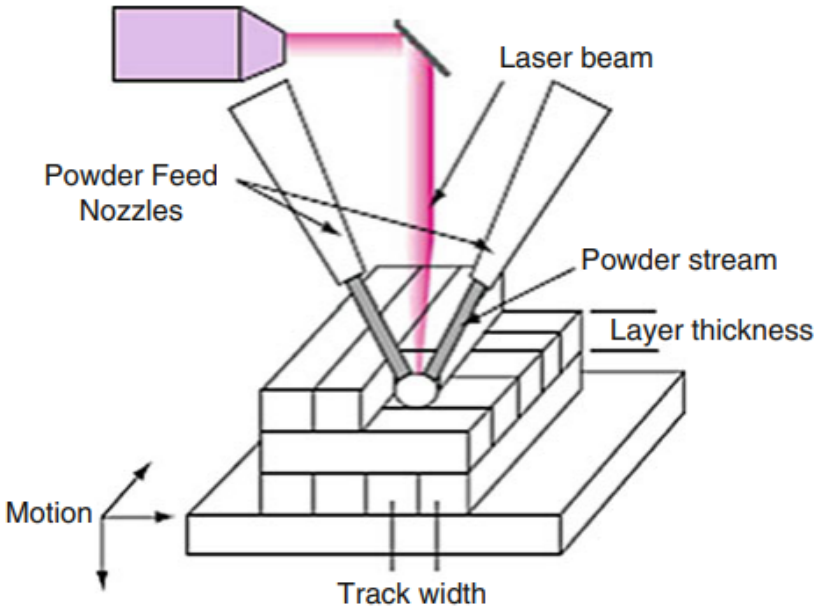

(a)

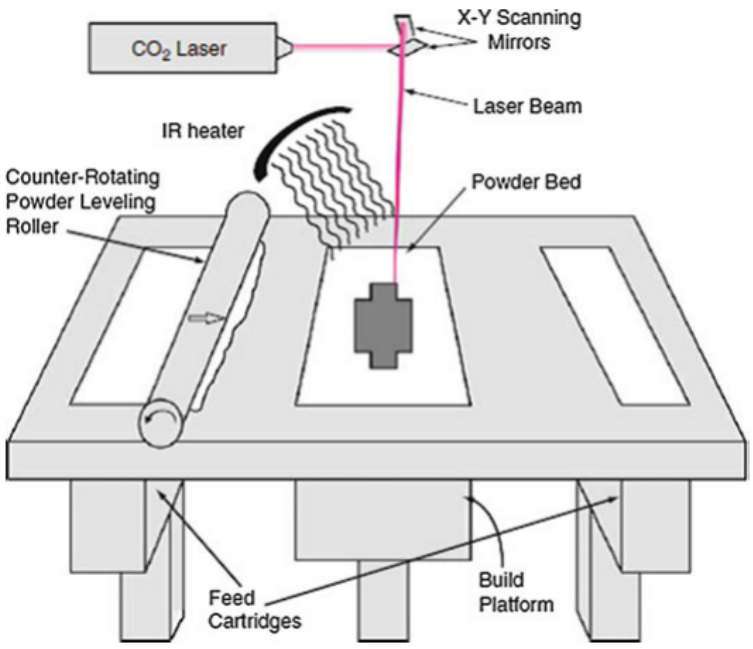

(b)

Figure 1.1: (a) Schematic of a typical laser powder Directed Energy Deposition process, (b) Schematic of a typical Powder Bed Fusion process, [1]

In laser-based AM processes for metallic parts, the resulting microstructure, residual stresses, and distortion are impacted by the molten pool where metal powder undergoes melting and solidification (phase change) and by repeated high energy heat source thermal cycles, which result in high temperature gradients, [4, 5, 6, 7, 8, 9]. In line with that, thermal analysis in additive manufacturing is interconnected (one-way coupled) with the mechanical and microstructural behavior, where the temperature distribution obtained during the process serves as input for the mechanical analysis, which predicts thermal stresses and strains in the component, as well as the microstructural evolution model. As a result, the thermal analysis can be conducted independently and the resulting temperature field can be subsequently utilized. It is evident that determining the thermal history produced in AM is essential for the overall analysis, and in this thesis, we present a three-dimensional model that numerically determines the temperature distribution of laser-based AM processes using metal powder, applicable to various process conditions.

Modeling of the AM process shares many similarities with multipass welding [10, 11], with the main distinction being that in AM, the size of the material deposited is significantly larger. The Finite Element Method (FEM) is used to model and simulate the thermal behavior of the system [12]. The two main material deposition models in the literature (1) quiet and (2) inactive elements [13], are investigated and a modification is implemented in the model in order to avoid errors and reduce computational cost. Appropriate convective and radiant boundary conditions are applied at each free surface during element activation, as neglecting these conditions, which is a common practice in welding modeling literature, has been demonstrated to lead to errors [14]. It is also crucial to take into account latent heat effects caused by phase changes (i.e., melting and solidification) in the analysis, since the metal powder melts quickly around the heat source forming, the molten pool [15]. In this analysis complex physical phenomena and mass transport in molten pool [16], are simplified and its effects are implemented into the simulation by a distributed heat input model [17] and forced convection [18] in the heat affected zone. In this thesis, the FEM software ABAQUS [19] is employed, to simulate the thermal behavior of a three-dimensional laser-based AM process for metallic parts [20, 21, 22] and calculate the temperature field.

Chapter 2 of this thesis provides a comprehensive presentation of the theoretical formulation of thermal analysis in the context of additive manufacturing. It elaborates the fundamental principles underlying thermal analysis and how these principles are applied to additive manufacturing. Chapter 3 focuses on the modeling of the AM process using the finite element method. The chapter provides a detailed description of the process of developing a numerical model of the AM process. To this end, specialized ABAQUS subroutines are implemented to simulate the thermal behavior of the system. These subroutines take into account the power of the heat source, the melting and solidification of the metal powder, the movement of the laser beam and the convective and radiant boundary condition at every free surface, among other factors. According to the general model that was developed in Chapters 2 and 3, a detailed simulation of the three-dimensional AM process is performed for an AISI 316L stainless steel. The results of the analysis provide useful information about the thermal history and temperature field and verify that the model accurately simulates the process.

Chapter 2

Theoretical formulation of thermal analysis in additive manufacturing

2.1 Theory

In this section a comprehensive overview of the fundamental principles and mechanisms of heat transfer is presented [23, 24]. Heat is a form of energy that is transferred from one system to another as a result of a difference in temperature. Heat transfer can be steady or transient. In steady heat transfer the heat transferred through a medium is constant, while in transient heat transfer the temperature distribution in a medium changes continuously with time until a steady state is reached. There are three fundamental mechanisms of heat transfer, which are conduction, convection, and radiation. Additionally heat generation and phase change highly influence the overall heat transfer process.

2.1.1 Heat conduction

Heat conduction is the transfer of heat energy from one molecule to another within a material, or from one material to another in contact, due to a difference in temperature.
The rate of heat conduction through a medium depends on the geometry of the medium, its thickness, and the material of the medium, as well as the temperature difference across the medium. If the heat conduction is significant in one direction and negligible in the others, the heat transfer is called 1-dimensional and the rate of heat flow ($\dot{Q}_{cond}$) is described by the 1-dimensional Fourier's law of heat conduction :

$$\dot{Q}_{cond} = -k\,A\left(\frac{dT}{dx}\right) \qquad (W) \tag{2.1}$$

- k is the thermal conductivity of the material ($\frac{W}{m\,K}$)
- A is the cross-sectional area (m^2)

- $\frac{dT}{dx}$ is the temperature gradient $(\frac{K}{m})$

The negative sign in Eq.(2.1) ensures that the heat flow is in the direction of decreasing temperature, as heat always flows from higher to lower temperatures.
The ability of a material to conduct heat is referred as its thermal conductivity. It is influenced by various factors such as the microstructure and temperature of the material. In anisotropic materials, the thermal conductivity is expressed as a second-order tensor (k_{ij}) which reflects the varying conductive heat transfer in different directions. Conversely, isotropic materials have the same properties in all directions and are homogeneous, leading to a scalar value (k) representing the overall conductive heat transfer in the material, since the thermal conductivity tensor is equal in all directions.
Considering a 3-dimensional temperature distribution in an isotropic material, the general relation for Fourier's law of heat conduction can be written as :

$$\vec{q} = -k(T)\,\nabla T \qquad \left(\frac{W}{m^2}\right) \tag{2.2}$$

Where $\vec{q}$ is the heat flux vector, $k(T)$ is the temperature dependent thermal conductivity of the material, and ∇T is the temperature gradient. The negative sign indicates that heat flows from higher temperature to lower temperature.
In component form, the Eq.(2.2) can be written as:

$$q_x = -k(T)\,\frac{\partial T}{\partial x} \qquad q_y = -k(T)\,\frac{\partial T}{\partial y} \qquad q_z = -k(T)\,\frac{\partial T}{\partial z} \qquad \left(\frac{W}{m^2}\right) \tag{2.3}$$

$$\vec{q} = q_x\,\vec{i} + q_y\,\vec{j} + q_z\,\vec{k} \tag{2.4}$$

Where q_x, q_y, and q_z are the components of the heat flux vector in the x, y, and z directions, respectively, $\vec{i}$,$\vec{j}$ and $\vec{k}$ are the unit vectors and $\frac{\partial T}{\partial x}$, $\frac{\partial T}{\partial y}$, and $\frac{\partial T}{\partial z}$ are the partial derivatives of temperature with respect to x, y, and z, respectively.

2.1.2 Heat convection

Convection is the mode of energy transfer between a solid surface and the adjacent liquid or gas that is in motion, and it involves the combined effects of conduction and fluid motion. Unlike heat conduction, which occurs through direct contact between two bodies, heat convection involves the transfer of heat by the motion of a fluid, such as air or water. Convective heat transfer increases with higher fluid speed.
Heat convection can be either natural (free) or forced. Natural convection occurs when the

fluid motion is caused by the buoyancy forces that are induced by the temperature difference in the fluid. In contrast forced convection occurs when the fluid is forced to flow over the surface by external means, such as a fan, pump, or wind.
Heat transfer by convection can be complicated because the fluid motion and temperature distribution are not always uniform and predictable. However the rate of heat transfer between a body and its surroundings is proportional to the temperature difference between them. For natural convention the rate of heat transfer $\dot{Q}_{conv}$ is expressed by Newton's law of cooling as :

$$\dot{Q}_{conv} = h\,A\,(T_s - T_\infty) \qquad (W) \tag{2.5}$$

- h is the heat transfer coefficient $(\frac{W}{m^2\,K})$
- A is the surface area (m^2)
- T_s is the temperature of the surface (K)
- T_∞ is the temperature of the surroundings (K)

The convection heat transfer coefficient h is a measure of the effectiveness of the interface between the fluid and the surface and it is important in determining the rate of heat transfer through convection. It is important to mention that is not a property of the fluid. It is an experimentally determined parameter whose value depends on all the variables influencing convection such as the surface geometry, the nature of fluid motion, the properties of the fluid, and the bulk fluid velocity.

2.1.3 Radiation

All bodies constantly emit energy by a process of electromagnetic radiation.The intensity of this radiant energy flux depends upon the temperature of the body and the nature of its surface. The full electromagnetic spectrum includes an enormous variety of energy-bearing waves, of which heat is only a small part. In heat transfer, thermal radiation is involved, which is the form of radiation emitted by bodies because of their temperature. It differs from other forms of electromagnetic radiation such as x-rays, gamma rays, microwaves, radio waves, and television waves that are not related to temperature. All bodies at a temperature above absolute zero emit thermal radiation. Unlike conduction and convection, the transfer of energy by radiation does not require the presence of an intervening medium.
Despite radiation being a volumetric phenomenon, it is usually considered to be a surface phenomenon for solids that are opaque to thermal radiation such as metals, wood, and rocks since the radiation emitted by the interior regions of such material can never reach the surface. A black body is the theoretical model for the perfect thermal radiator, a body that absorbs all energy that reaches it and reflects nothing. The rate of radiation $(\dot{Q}_{rad})$ emitted

from a black body reaches a theoretical maximum, which is given by the Stefan-Boltzmann law :

$$\dot{Q}_{rad} = \sigma\, A\, T^4 \qquad (W) \tag{2.6}$$

Where:

- σ is the Stefan-Boltzmann constant (5.67 x 10^{-8} $\frac{W}{m^2\, K^4}$)
- A is the surface area of the blackbody (m^2)
- T is the absolute temperature of the blackbody (K)

The radiation emitted by all real surfaces is less than the radiation emitted by a black body at the same temperature, and is expressed by a modified version of Eq.(2.6) as:

$$\dot{Q}_{rad} = \epsilon\, \sigma\, A\, T^4 \qquad (W) \tag{2.7}$$

Where (ϵ) is the emissivity factor of the surface. Real surfaces can be considered as grey bodies because they don't emit or absorb radiation at the maximum possible rate. The emissivity factor varies between 0 and 1, with 1 for a black body and 0 for a body that reflects all incident radiation. The emissivity of real surfaces depends on their composition, surface roughness, and temperature.
Absorptivity (α) is the ratio of the energy absorbed by a material to the energy incident upon it. It is a measure of the ability of a material to absorb radiation and is expressed as a dimensionless value between 0 and 1. The relationship between absorptivity and emissivity is expressed by Kirchhoff's law of thermal radiation, which states that the emissivity and absorptivity of a body are equal for all wavelengths at a given temperature, $\epsilon = \alpha$.
If $\dot{Q}_{incident}$ denotes the rate at which radiation is incident on the surface and α is the absorptivity of the surface, then the rate at which a surface absorbs and reflects radiation is determined, respectively, as:

$$\dot{Q}_{abs} = \alpha\, \dot{Q}_{incident} \tag{2.8}$$

$$\dot{Q}_{refl} = (1 - \alpha)\, \dot{Q}_{incident} \tag{2.9}$$

The net radiation heat transfer is calculated as the difference between the amount of radiation emitted by a surface and the amount absorbed. If the surface absorbs more radiation than

it emits, it is considered to be gaining energy through radiation. Conversely, if it emits more radiation than it absorbs, it is considered to be losing energy.
When a surface of emissivity ϵ and surface area A at an absolute temperature T is completely enclosed by a much larger (or black) surface at absolute temperature T_{surr} separated by air (or any other gas that does not intervene with radiation), the net rate of radiation heat transfer is given by:

$$\dot{Q}_{rad} = \epsilon\,\sigma\,A\,(T^4 - T_{surr}^4) \qquad (W) \tag{2.10}$$

In this particular case, the net radiation heat transfer is not influenced by either the emissivity or the surface area of the surrounding surfaces.

2.1.4 Heat Generation

The process by which thermal energy is created or added to a system is called heat generation and it is a fundamental concept in thermodynamics. It is a process by which energy is converted from one form to another, resulting in an increase in temperature. Heat generation can occur due to a variety of mechanisms such as electrical resistance, chemical reactions, friction, and radioactive decay.
Heat generation can be represented mathematically by the first law of thermodynamics, also known as the law of conservation of energy. This law states that the change in internal energy of a closed system is equal to the heat added to the system, minus the work done by the system. The mathematical equation for the first law of thermodynamics is:

$$\Delta U = Q - W \tag{2.11}$$

Where ΔU is the change in internal energy, Q is the heat added to the system, and W is the work done by the system. It is important to note that this equation is only valid for closed systems, where no mass is exchanged with the surroundings. In open systems, the change in internal energy also includes the heat and work exchanged with the surroundings.
In addition to the first law of thermodynamics, heat generation can also be represented by the heat generation rate.Note that heat generation is a volumetric phenomenon. That is, it occurs throughout the body of a medium. Therefore, the rate of heat generation in a medium is usually specified per unit volume and is denoted by $\dot{q}_{gen}$ in $\left(\frac{W}{m^3}\right)$. The rate of heat generation in a medium may vary with time as well as position within the medium. When the variation of heat generation with position is known, the total rate of heat generation in a medium of volume V can be determined from:

$$\dot{Q}_{gen} = \int_V \dot{q}_{gen}\,\mathrm{d}V \qquad (W) \tag{2.12}$$

2.1.5 Internal energy and latent heat

The energy associated with the molecular structure and activity within a system is referred to as microscopic energy. The sum of all microscopic forms of energy is called the internal energy of a system. The rate equation for the internal energy per unit mass of a system is expressed by:

$$\dot{U} = c\,\dot{T} \qquad \left(\frac{W}{kg}\right) \tag{2.13}$$

Where:

- U is the internal energy per unit mass $\left(\frac{J}{kg}\right)$
- c is the temperature dependent specific heat, $c(T) = \frac{\partial U(T)}{\partial T}$, $\left(\frac{J}{kg\,K}\right)$
- T is temperature (K)

The internal energy is also associated with the intermolecular forces between the molecules of a system. If sufficient energy is added to the molecules of a solid or liquid, they will overcome these molecular forces and simply break away, turning the system to a gas. This is a phase change process and because of this added energy, a system in the gas phase is at a higher internal energy level than it is in the solid or the liquid phase. The internal energy associated with the phase of a system is called latent heat.
Latent heat is important in the understanding of phase changes in metals and alloys. Latent heat of solidification is the heat energy required to change a metal from the liquid state to the solid state at a constant temperature, while latent heat of fusion (melting) is the heat energy required to change a metal from the solid state to the liquid state at a constant temperature.
Overall, when the material changes phase, there is an extra change in the internal energy caused by the latent heat effects. In this case Eq.(2.14) is written as:

$$\dot{U} = c\,\dot{T} + \dot{U}_l \qquad \left(\frac{W}{kg}\right) \tag{2.14}$$

Where $\dot{U}_l$ is the internal energy per unit mass associated with melting and solidification.

- $\dot{U}_l > 0$ when the material absorbs energy (melting)

- $\dot{U}_l < 0$ when the material releases energy (solidification)

The latent heat U_{latent} is assumed to be absorbed or released over a range of temperatures from a lower (solidus) temperature T_S to an upper (liquidus) T_L temperature.

$$U_{latent} = U_l(T_L) - U_l(T_S) \tag{2.15}$$

The solidus temperature and liquidus temperature are important concepts in materials science and metallurgy that describe the temperature range in which a material is in a partially solid and partially liquid state. The solidus temperature marks the transition from the solid state to the partially solid and partially liquid state and is defined as the temperature below which a material is completely solid. The liquidus temperature marks the transition from the partially solid and partially liquid state to the completely liquid state and is defined as the temperature above which a material is completely liquid.
The internal energy per unit mass associated to latent heat $U_l(T)$ is assumed to vary smoothly from $U_l(T_S) = 0$ to $U_l(T_L) = U_{latent}$ according to:

$$U_l(T) = U_{latent}\left[3\left(\frac{T - T_S}{T_L - T_S}\right)^2 - 2\left(\frac{T - T_S}{T_L - T_S}\right)^3\right] \tag{2.16}$$

Where the cubic function above is chosen so that

$$\left.\frac{\mathrm{d}U_l}{\mathrm{d}T}\right|_{T=T_S} = \left.\frac{\mathrm{d}U_l}{\mathrm{d}T}\right|_{T=T_L} = 0 \tag{2.17}$$

2.1.6 General heat conduction equation

In order to model a general heat transfer problem, heat transfer must be considered in all directions. In such cases heat conduction is said to be multidimensional, and the governing differential equation in 3-dimensional systems in rectangular coordinate systems must be developed.
Consider a small rectangular element of length Δx, width Δy, and height Δz, as shown in Fig: 2.1. Assume the density of the body is ρ and the specific heat is c. An energy balance on this element during a small time interval Δz can be expressed as:

$$(\dot{Q}_x + \dot{Q}_y + \dot{Q}_z) - (\dot{Q}_{x+\Delta x} + \dot{Q}_{y+\Delta y} + \dot{Q}_{z+\Delta z}) + \dot{G}_{element} = \frac{\Delta E_{element}}{\Delta t} \tag{2.18}$$

Where

- $(\dot{Q}_x + \dot{Q}_y + \dot{Q}_z)$ is the rate of heat conduction at x, y and z.
- $(\dot{Q}_{x+\Delta x} + \dot{Q}_{y+\Delta y} + \dot{Q}_{z+\Delta z})$ is the rate of heat conduction at $x+\Delta x$, $y+\Delta y$ and $z+\Delta z$.
- $\dot{G}_{element}$ is the rate of heat generation inside the element.
- $\frac{\Delta E_{element}}{\Delta t}$ is the rate of change of the energy content of the element,

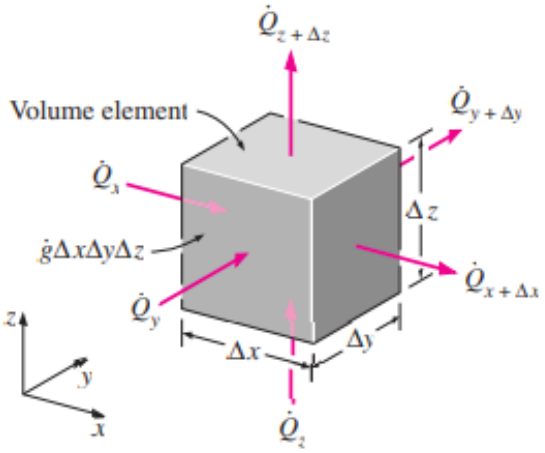

Figure 2.1: Three-dimensional heat conduction through a rectangular volume element, Retrieved from [24]

Noting that the volume of the element is $V_{element} = \Delta x\, \Delta y\, \Delta z$, the change in the energy content of the element and the rate of heat generation within the element can be expressed as:

$$\frac{\Delta E_{element}}{\Delta t} = E_{t+\Delta t} - E_t = \rho\, c\, \Delta x\, \Delta y\, \Delta z\, (T_{t+\Delta t} - T_t) \tag{2.19}$$

$$\dot{G}_{element} = \dot{g}\, V_{element} = \dot{g}\, \Delta x\, \Delta y\, \Delta z \tag{2.20}$$

Substituting Eq.(2.14) and Eq.(2.20) into Eq.(2.18)

$$(\dot{Q}_x + \dot{Q}_y + \dot{Q}_z) - (\dot{Q}_{x+\Delta x} + \dot{Q}_{y+\Delta y} + \dot{Q}_{z+\Delta z}) + \dot{g}\,\Delta x\,\Delta y\,\Delta z = \\ = \rho\,c\,\Delta x\,\Delta y\,\Delta z\,\frac{T_{t+\Delta t} - T_t}{\Delta t} \tag{2.21}$$

Finally dividing Eq.(2.21) by $\Delta x\,\Delta y\,\Delta z$ gives:

$$-\frac{1}{\Delta y\,\Delta z}\,\frac{\dot{Q}_{x+\Delta x} - \dot{Q}_x}{\Delta x} - \frac{1}{\Delta x\,\Delta z}\,\frac{\dot{Q}_{y+\Delta y} - \dot{Q}_y}{\Delta y} - \frac{1}{\Delta x\,\Delta y}\,\frac{\dot{Q}_{z+\Delta z} - \dot{Q}_z}{\Delta z} + \dot{g} = \\ = \rho\,c\,\frac{T_{t+\Delta t} - T_t}{\Delta t} \tag{2.22}$$

Noting that the heat transfer areas of the element for heat conduction in the x, y, and z directions are respectively

$$A_x = \Delta y\,\Delta z, \quad A_y = \Delta x\,\Delta z, \quad A_z = \Delta x\,\Delta y$$

and taking the limit as

$$\Delta x, \Delta y, \Delta z \to 0 \quad \text{and} \quad \Delta t \to 0$$

Eq.(2.22) can be written as:

$$-\frac{1}{A_x}\,\frac{\partial Q_x}{\partial x} - \frac{1}{A_y}\,\frac{\partial Q_y}{\partial y} - \frac{1}{A_z}\,\frac{\partial Q_z}{\partial z} + \dot{g} = \rho\,c\,\frac{\partial T}{\partial t} \tag{2.23}$$

Implementing in Eq.(2.23) the general relation for Fourier's law of heat conduction Eq.(2.3) for heat transfer areas A_x, A_y, A_z, the general heat conduction equation in rectangular coordinates is expressed as :

$$\frac{\partial}{\partial x}\left(k\,\frac{\partial T}{\partial x}\right)\,\frac{\partial}{\partial y}\left(k\,\frac{\partial T}{\partial y}\right)\,\frac{\partial}{\partial z}\left(k\,\frac{\partial T}{\partial z}\right) + \dot{g} = \rho\,c\,\frac{\partial T}{\partial t} \tag{2.24}$$

The general heat conduction equation is a mathematical representation of the energy balance within a specific differential element of a medium. However, it should be noted that the equation itself is limited in scope, as it only considers the energy balance within the differential element and does not take into account any surface conditions, such as the surface temperature or a specified heat flux, that may be present. On top of that Eq.(2.24) is a Partial Differential Equation, thus the specification of both boundary and initial conditions is required in order to have a well-posed problem and obtain meaningful solutions.
More specifically, boundary conditions in heat transfer analysis describe the behavior of the temperature field at the boundaries of the system being studied.

- Dirichlet Boundary Conditions: These conditions specify the temperature at a given boundary S.

$$T(\vec{r}_S, t) = T_S(t) \tag{2.25}$$

- Neumann Boundary Conditions: These conditions specify the heat flux at a given boundary S.

$$\left.\frac{\partial T}{\partial n}\right|_S = q_n \tag{2.26}$$

Where $T(\vec{r}_S, t)$ is the temperature at a point of the boundary surface S, $T_S(t)$ is the specified temperature at the boundary surface S and q_n is the specified heat flux at a point on the boundary surface S, and it is positive when heat enters the body and negative when heat flows out of the body. In other words the value of q_n determines the heat transfer across the boundary surface, and its sign indicates the direction of heat transfer.
Additionally, in heat transfer analysis, initial conditions specify the temperature distribution within the system at a particular moment in time, mainly at time $t = 0$.

$$T(x, y, z, t_0) = T_0(x, y, z) \quad at \quad t = t_0 \tag{2.27}$$

Here, $T_0(x, y, z)$ is the initial temperature distribution within the system at time t_0.

2.2 Heat transfer in Additive Manufacturing

In this section, we present the mathematical formulation of heat transfer analysis as it relates to additive manufacturing techniques using metal powder and an energy source, such as a laser or electron beam, to fabricate parts through layer-by-layer building.
The general heat conduction equation Eq.(2.24) which represents the energy balance, without taking latent heat effects into account ($\dot{U} = c\dot{T}$) can be expressed as:

$$\nabla \cdot (k\,\nabla T) + \dot{g} = \rho\,\dot{U} \tag{2.28}$$

During the additive manufacturing process, the energy source (such as a laser or electron beam) heats the powder material, causing it to go through a phase change from solid to liquid. The melted material then cools and solidifies, bonding the powder particles together to form a solid layer. For that reason effects at phase change must be included in the analysis. By incorporating latent heat effects into the internal energy based on Eq.(2.14), Eq.(2.28) can be modified as follows:

$$\nabla \cdot (k\,\nabla T) + \dot{g} = \rho\,(c\,\dot{T} + \dot{U}_l) \tag{2.29}$$

Where $\dot{U}_l$ is the internal energy per unit mass associated with melting or solidification.
For homogeneous materials the governing equation is expressed as:

$$k\,\nabla^2 T + (\dot{g} - \rho\,\dot{U}_l) = \rho\,c\,\dot{T} \tag{2.30}$$

Where:

- ρ is the mass density of the material ($\frac{kg}{m^3}$)
- $k = k(T)$ is the temperature dependent thermal conductivity ($\frac{W}{m\,K}$)
- $c = c(T)$ is the temperature dependent specific heat ($\frac{J}{kg\,K}$)
- $\dot{g}$ is the heat generation caused by the energy source (laser) ($\frac{W}{m^3}$)
- U_l is the internal energy associated with phase change ($\frac{J}{kg}$)
- T is temperature (K)

It is important to include accurate boundary conditions on the free surfaces (S) of the model. The heat transfer across these surfaces is assumed to occur through both convection Eq.(2.5) and radiation Eq.(2.10), and the resulting heat flux at each boundary is specified by Eq.(2.26).

$$q_n = -h\,(T - T_{surr}) - \epsilon\,\sigma\,(T^4 - T_{surr}^4) \tag{2.31}$$

Where T_{surr} represents the temperature of the surrounding environment. It is crucial to remember that all temperature values must be expressed in Kelvin (K) due to the presence of the fourth power in the equation that represents thermal radiation.

Chapter 3

Finite element modeling of Additive Manufacturing

3.1 Laser scanning strategy and heat source model

To simulate the thermal history of the additive manufacturing process, a 3-dimensional model was developed in ABAQUS [19], a software that is used for finite element analysis (FEA) and computer-aided engineering (CAE).
For this work a simple laser scanning path is simulated to design a cuboid object based on a bigger substrate. More specifically, the laser scans across the x-axis in parallel rows, returning to the starting point after each one, but slightly shifted on the z-axis (dz) to scan the next row (hatching space). This process continues until a complete layer in the x-z plane is scanned. The laser then moves upward on the y-axis, by a parameter called layer thickness, to begin scanning the next layer. This process is repeated until the final object is created, as seen in figure 3.1
It is important to acknowledge that the laser is only active during movement on the x-axis, where it prints a thin row of material as it scans. Each row is completed through a single scan and there is a brief period of inactivity (idle time) for the system to cool down after each x-axis pass and after each layer in the x-z plane has been finished.
A user-defined subroutine was created to calculate the location of the laser beam center $(x^{laser}, y^{laser}, z^{laser})$ at each time increment that the laser was active, based on the previously defined scanning pattern. During periods of inactivity, the laser position was reset to the starting position for the subsequent scan.

The heat input from the laser onto the part in additive manufacturing is simulated by a double ellipsoid volumetric heat source input model [17]. This heat source model is composed of two concentric ellipsoids with semi-axes lengths (a_1, b_1, c_1) and (a_2, b_2, c_2) and center points (x_1, y_1, z_1) and (x_2, y_2, z_2) in 3-D space. For this work, to simplify the analysis, same semi-axes lengths (a, b, c) and same center points $(x^{\text{laser}}, y^{\text{laser}}, z^{\text{laser}})$ are considered.
The local coordinates referenced at the center of the ellipsoid were calculated. The local coordinates for the analysis are defined as the difference between the coordinates of the center of the laser source and the coordinates of an integration point. An integration point

is the point within an element at which integrals are evaluated numerically in finite element analysis.

- $\xi = x^{\text{laser}} - x^{\text{npt}}$
- $\eta = y^{\text{laser}} - y^{\text{npt}}$
- $\zeta = z^{\text{laser}} - z^{\text{npt}}$

The heat flux of the 3-D ellipsoid volumetric heat source model can be calculated as:

$$\dot{g} = \frac{6\,P}{a\,b\,c\,\pi}\,\exp\left[-3\left(\frac{\xi^2}{a^2}+\frac{\eta^2}{b^2}+\frac{\zeta^2}{c^2}\right)\right] \tag{3.1}$$

Where :

- $\dot{g}$ is the power density of the heat source $(\frac{W}{mm^3})$
- P is the energy input rate of the heat source (W).
- (a, b, c) are the semi-axes lengths of the ellipsoid (mm).
- (ξ, η, ζ) are the local coordinates as defined above (mm).

The heat generated by the laser beam, as modeled in Eq.(3.1), is reflected in the heat generation term, $\dot{g}$, in Eq.(2.30).

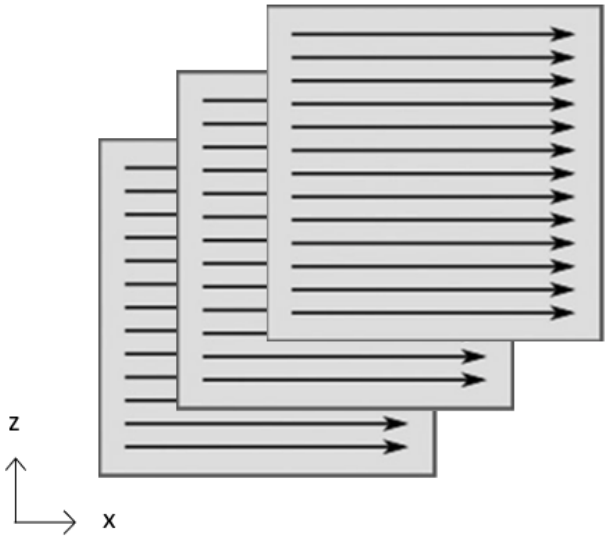

Figure 3.1: Laser scanning path.

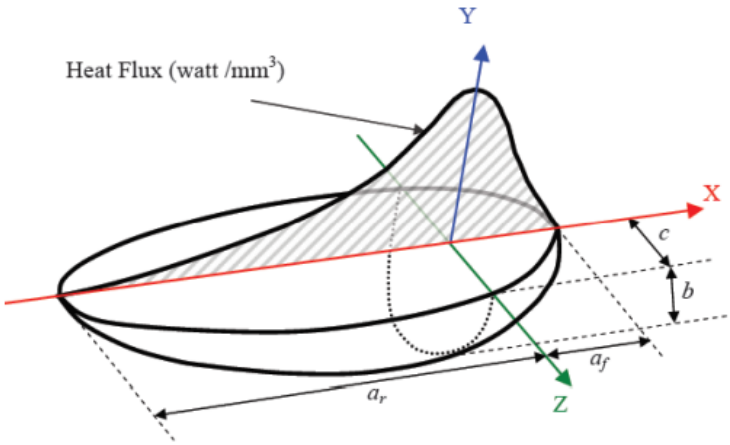

Figure 3.2: Goldak's double ellipsoidal heat source model [25].

3.2 Material deposition modeling

In this section the two main methods used in the literature for modeling material deposition in finite element analyses [13, 14] are described.

1. The quiet element method
2. The inactive element method

Then a modified method that uses ABAQUS user subroutine *MPC is introduced.

3.2.1 Quiet element method

The quiet element method is a numerical technique used to model material deposition in additive manufacturing processes. In this method, the elements representing the metal deposition regions are included from the beginning of the analysis, but they are assigned specific properties that minimize their influence on the overall analysis. Specifically, for heat transfer analyses, the thermal conductivity of the quiet elements is set to a lower value to reduce conduction into these regions, and the specific heat is also adjusted to a lower value to minimize energy transfer to these elements.
The thermal conductivity and specific heat used for the quiet elements, denoted by k_{quiet} and c_{quiet}, respectively, are defined as a scaled version of the thermal conductivity k and specific heat c of the base material. The scaling factors, s_k and s_c, are utilized to adjust the thermal conductivity and specific heat of the quiet elements, respectively.

$$k_{quiet} = s_k \cdot k \tag{3.2}$$

$$c_{quiet} = s_c \cdot c \tag{3.3}$$

The quiet element method can easily be integrated into existing commercial finite element software using user-defined subroutines, but the determination of the appropriate magnitude of the scaling factors constitutes a significant challenge, as deviations from optimal values can result in errors. Furthermore, if the scaling factors are overly small, it may result in an ill-conditioned system of equations. In the context of finite element analysis (FEA), a system of equations is considered ill-conditioned if it is sensitive to small changes in the input data. In other words, small changes in the input can result in large changes in the output. This can make it difficult to obtain accurate solutions to the system of equations and can also lead to numerical instability when solving the system using iterative methods.

3.2.2 Inactive element method

The inactive element method initially excludes the elements that represent material deposition from the analysis until they are activated. In that manner only active elements are considered in the analysis. In the inactive element method the activation of new elements can introduce artificial thermal energy generation in the system as a result of shared nodes between active and inactive elements. An effective solution to this problem is to set the temperature of shared nodes, those between activated and soon-to-be activated elements, to the initial temperature. This method has been demonstrated to eliminate artificial thermal energy generation during element activation. Overall this method is more complicated and thus cannot be easily integrated into finite element software using user-defined subroutines.

3.2.3 Modified quiet element method

In this study, a variation of the quiet element technique is used to simulate material deposition with the implementation of ABAQUS subroutine *MPC. Generally, *MPC is called to impose a user-defined multi-point constraint, and in this work it is used to maintain the nodal temperature of inactive elements at the same level as their initial temperature.
More specifically, as with the quiet element method, the elements representing the metal deposition regions are included from the start of the analysis. For inactive elements the scaling factors for thermal conductivity and specific heat in equations 3.2 and 3.3 are set to zero ($s_k = s_c = 0$) to ensure that they will not impact the analysis. At the start of the simulation, the temperature of each node that represents a part of the material deposition region is set to match that of a selected reference node on the substrate, which always maintains the initial temperature. Once the process starts and the laser beam begins scanning, this subroutine calculates the distance of each integration point from the center of the heat source for every time increment. If an integration point of an inactive element falls within the three-dimensional ellipsoid of the heat source, the element is activated and the temperatures of its nodes are no longer subject to the constraint imposed earlier.
By using this approach, errors caused by scaling factors and artificially generated heat energy in the quiet and inactive element method respectively are avoided, while the method remains efficient and easy to implement in finite element analyses.

3.3 Element activation modeling

When an element is inactive, the first step in the activation process is to determine whether it should be activated. This is done by checking the location of its integration point in the current scanning layer (x-z plane). If the integration point satisfies the following conditions:

- $\eta \geq tol$ (where $tol = 10^{-4}$), situated in the current scanning layer
- $|\zeta| \leq c$ and $|\xi| \leq a$, situated within the boundaries of the ellipsoid in that layer

The element is activated and the interface between active and inactive elements is updated accordingly.

3.4 Modeling the interface between active and inactive elements

Applying the correct boundary conditions for convection and radiation at every free surface of the manufactured product is very important because it ensures that the results of the analysis accurately reflect the actual conditions present during the manufacturing process.
Free surfaces refer to the external perimeter of the product and to the evolving interface between active and inactive elements. The interface between active and inactive elements continuously changes during the material deposition, which makes it complicated to apply surface boundary conditions for convection and radiation, especially in 3 dimensional analyses. In multi-pass welding modeling simplifying the analysis by neglecting the interface is common and does not lead to errors since the size of the deposited material is minor compared to the substrate. On the contrary in the thermal analysis of additive manufacturing the size of the deposited material is considerably larger than multi-pass welding and this simplification can lead to significant errors, specifically to higher temperatures for ignoring heat losses due to convection and radiation.
For that reason in this work an algorithm that determines the faces of the elements that are exposed to convection and radiation for every time increment based on the history of the process, was developed and implemented in the 3 dimensional analysis.
Firstly element faces are defined (figure 3.3).

- Positive y-axis is referred to as top and negative y-axis is referred to as bottom of the element:
  - Face 5 refers to the top of the element
  - Face 3 refers to the bottom of the element

- Positive x-axis and positive z-axis are referred to as right and negative x-axis and negative z-axis respectively as left of the element:
  - Face 1 refers to the left of the element in relation to the z-axis
  - Face 2 refers to the right of the element in relation to the z-axis
  - Face 4 refers to the right of the element in relation to the x-axis
  - Face 6 refers to the left of the element in relation to the x-axis

To check if a surface of an element is an external free surface, thus boundary conditions for convection and radiation must be applied at that face, the first step is to check if the element is activated.

- For an element that was inactive and was activated at that time increment
  - If $|\eta| < dy$, then boundary conditions are applied at the Face 5 of the element.
  - If simultaneously $z^{npt} < {z_L}^0 + dz$, then the element belongs in the initial row of the layer and boundary conditions are applied at the Face 1 too.
  - If $z^{npt} > z_L + c - dz$ boundary conditions must be applied at the Face 2 of the element.
  - If $dx - \xi > a$ boundary conditions must be applied at the Face 4 of the element.
  - If $x^{npt} < {x_L}^0 + dx$ boundary conditions must be applied at the Face 6 of the element, because it is the first element of the corresponding row.
- For an element that was already activated in a specific time increment :
  - Boundary conditions are applied at Face 1 if the element belongs in the initial row of a layer, therefore $z^{npt} < {z_L}^0 + dz$
  - If the element is situated in the last row of a layer ($z^{npt} > (n_{rows} - 1)\, dz + {z_L}^0$) and at the same time that layer is under the layer that is currently manufactured ($\eta > dy$), boundary conditions must be applied at the Face 2.
    Also if the element belongs in the upper layer that is currently scanned ($|\eta| \leq dy$), there are two cases in which the Face 2 of an element can be a free surface. The first is that it belongs in the row that is currently scanned $dz - \zeta \geq c$. The second is that it belongs in the exact previous row ($z^{npt} < z_L$ and $2\, dz - \zeta \geq c$) and at the same time its position in the row regarding the x-axis is after the last activated element of the following row $x^{npt} > x_L + a$.
  - If the already activated element is the first element of a row $x^{npt} < x_L^0 + dx$ boundary conditions must be applied at the Face 6.

– Boundary conditions at Face 4 must be applied at an activated element if it is the last element of a row $x^{npt} > (n-1)\,dx + {x_L}^0$.
In the case of the row that is currently scanned, $z^{npt} \geq z_L$, if ($|\xi| + dx > a$ and $|\eta| < dy$) this is the last activated element of the row of the last layer and boundary condition are applied at Face 4.

– If the element is situated at the upper layer that is currently scanned $|\eta| < dy$ boundary conditions must be applied at Face 5.
If the element is situated at the exact previous layer $|\eta| < 2\,dy$, the check for the application of boundary conditions at the Face 5 is carried out in 2 sub-cases. If the activated element is situated on the right side of the row that is manufactured $z^{npt} > z_L + c$, boundary conditions must be applied at Face 5. If it is situated at the exact row of elements that the laser is scanning, ($z^{npt} > z_L$ and $z^{npt} < z_L + c$), and the exactly of above element is not yet activated $x^{npt} > x_L + a$, boundary conditions must be also applied at Face 5.

Where (x_L^0, y_L^0, z_L^0) are the initial coordinates of the laser, n_{rows} is the number or rows (elements in the z direction), n_{layers} is the number or layers (elements in the y direction) and n is the number of elements in the x direction.

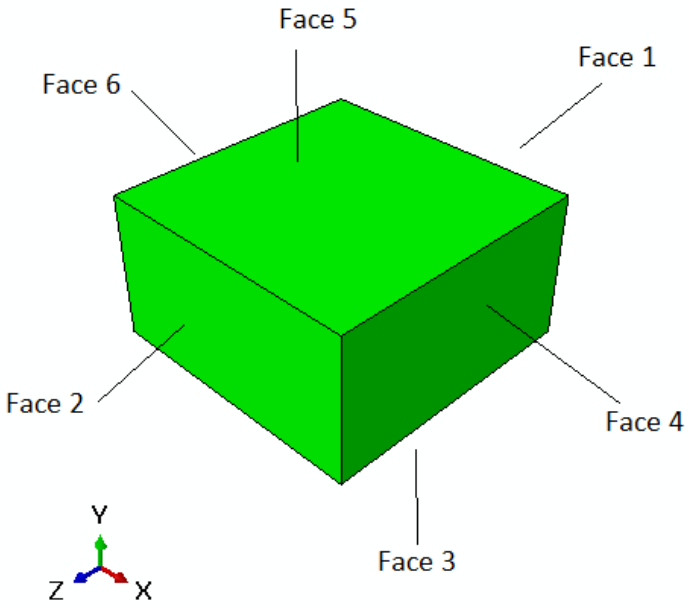

Figure 3.3: Element faces.

3.5 Heat transfer model in ABAQUS

The heat transfer model developed in section 2.2 is resolved by using the finite elements method in the Abaqus software, in order to calculate the temperature field during the process. The solution of the nonlinear heat transfer problem is developed incrementally. The *DFLUX and *UMATHT user subroutines are utilized for this reason [20, 21, 22].

3.5.1 Body and surface heat flux calculation with DFLUX

User subroutine DFLUX is used to define a nonuniform distributed flux as a function of position, time, temperature, element number and integration point number in heat transfer analysis.

Listing 3.1: User subroutine DFLUX interface

```
      SUBROUTINE DFLUX(FLUX,SOL,KSTEP,KINC,TIME,NOEL,NPT,COORDS,
     1 JLTYP,TEMP,PRESS,SNAME)
C
      INCLUDE 'ABA_PARAM.INC'
C
      DIMENSION FLUX(2), TIME(2), COORDS(3)
      CHARACTER*80 SNAME

       user coding to define FLUX(1) and FLUX(2)

      RETURN
      END
```

In Listing 3.1, FLUX(1) represents the magnitude of the heat flow onto the model at a specific point. This value is then passed into the routine as the magnitude of the flux specified as part of the element-based or surface-based flux definition.
FLUX(2) denotes the rate of change of the flux with respect to the temperature at this point.

The convective and radiant boundary conditions (Eq.(2.31)) on every free surface, including the evolving interface between active and inactive elements as modeled in section 3.4, are simulated in FLUX(1) as part of the surface-based flux, within the user subroutine *DFLUX. It is important to include the effects of the heating zone and the molten pool into the simulation. In additive manufacturing the heating zone refers to the area where the material is heated in order to reach its melting temperature, allowing it to solidify and adhere to the previous layer. The material is melted within the heating zone to form a liquid or semi-liquid pool, also known as the molten pool. Heat transfer through mass transport in the melt pool is not directly simulated in this work. Instead the gas and powder flow near the heating zone is simulated as a forced convection region moving along with the heat source. This

region has a spherical shape with 5 mm radius and the convective heat transfer coefficient is 21 times the one that is used in free convection regions $H = 21\,h$. A user subroutine is developed to calculate the distance of each integrartion point from the center of the heat source. If an integration point is situated within the 5 mm radius from the center of the heat source and belongs to an activated element with a free surface, the heat transfer coefficient for forced convection H is used to simulate the boundary conditions in FLUX(1).

The heat source of the laser beam and the effects of the latent heat to the internal energy, $\dot{g}$ and $\rho\,\dot{U}_l$ respectively in Eq.(2.30) are also modeled with the user subroutine *DFLUX, this time simulated in FLUX(1) as part of the element-based (body) flux.
To determine $\dot{g}$, Eq.(3.1) is modeled and used in *DFLUX when the laser beam is active.
To determine $\rho\,\dot{U}_l$ in order to be implemented in *DFLUX, a user subroutine is developed, that defines the rate of body heat per unit volume $r_l = \rho\,\dot{U}_l$ at every integration point within each time increment and the variation of r_l with respect to temperature, $\frac{dr_l}{dT}$.
Let $[T_n, T_{n+1}]$ be the temperature increment during the time increment $[t_n, t_{n+1}]$. Two cases are distinguished:

a) **Melting** ($T_n < T_{n+1}$)**:** when melting takes place, the material absorbs energy ($\dot{U}_l > 0$). Latent heat is absorbed over the range T_S to T_L. Depending on the temperature increment under consideration, we distinguish the cases presented in Table 3.1.

b) **Solidification** ($T_n > T_{n+1}$)**:** when solidification takes place, the material releases energy ($\dot{U}_l < 0$). Latent heat is released over the range T_L to T_S. Depending on the temperature increment under consideration, we distinguish the cases presented in Table 3.2.

The cases displayed in Tables 3.1 and 3.2 along with material information such as density ρ, latent heat U_{latent}, and solidus and liquidus temperatures T_s, T_L are integrated into the user subroutine to determine $r_l = \rho\,\dot{U}_l$ and $\frac{dr_l}{dT}$ at every integration point for each time increment.

Case	Heat flux	Heat flux change per temperature
$T_n < T_{n+1} \leq T_S$	$r_l = 0$	$\frac{\mathrm{d}r_l}{\mathrm{d}T} = 0$
$T_n \leq T_S \leq T_{n+1} \leq T_L$	$r_l = -\frac{U_l\vert_{n+1}}{\Delta T}$	$\frac{\mathrm{d}r_l}{\mathrm{d}T} = -\frac{1}{\Delta T}\ \frac{\mathrm{d}U_l}{\mathrm{d}T}\big\vert_{n+1}$
$T_n \leq T_S < T_L \leq T_{n+1}$	$r_l = -\frac{U_{latent}}{\Delta T}$	$\frac{\mathrm{d}r_l}{\mathrm{d}T} = 0$
$T_S \leq T_n < T_{n+1} \leq T_L$	$r_l = -\frac{U_l\vert_{n+1} - U_l\vert_n}{\Delta T}$	$\frac{\mathrm{d}r_l}{\mathrm{d}T} = -\frac{1}{\Delta T}\ \frac{\mathrm{d}U_l}{\mathrm{d}T}\big\vert_{n+1}$
$T_S \leq T_n \leq T_L \leq T_{n+1}$	$r_l = -\frac{U_{latent} - U_l\vert_n}{\Delta T}$	$\frac{\mathrm{d}r_l}{\mathrm{d}T} = 0$
$T_L \leq T_n < T_{n+1}$	$r_l = 0$	$\frac{\mathrm{d}r_l}{\mathrm{d}T} = 0$

Table 3.1: Cases distinguished depending on the temperature increment when melting takes part, ($\Delta T = T_{n+1} - T_n$), [10]

Case	Heat flux	Heat flux change per temperature
$T_L \leq T_{n+1} < T_n$	$r_l = 0$	$\frac{\mathrm{d}r_l}{\mathrm{d}T} = 0$
$T_S \leq T_{n+1} \leq T_L \leq T_n$	$r_l = \frac{U_{latent} - U_l\vert_{n+1}}{\Delta T}$	$\frac{\mathrm{d}r_l}{\mathrm{d}T} = -\frac{1}{\Delta T}\ \frac{\mathrm{d}U_l}{\mathrm{d}T}\big\vert_{n+1}$
$T_S \leq T_{n+1} < T_n \leq T_L$	$r_l = \frac{U_l\vert_n - U_l\vert_{n+1}}{\Delta T}$	$\frac{\mathrm{d}r_l}{\mathrm{d}T} = -\frac{1}{\Delta T}\ \frac{\mathrm{d}U_l}{\mathrm{d}T}\big\vert_{n+1}$
$T_{n+1} \leq T_S < T_L \leq T_n$	$r_l = \frac{U_{latent}}{\Delta T}$	$\frac{\mathrm{d}r_l}{\mathrm{d}T} = 0$
$T_{n+1} \leq T_S \leq T_n \leq T_L$	$r_l = \frac{U_l\vert_n}{\Delta T}$	$\frac{\mathrm{d}r_l}{\mathrm{d}T} = 0$
$T_{n+1} < T_n \leq T_S$	$r_l = 0$	$\frac{\mathrm{d}r_l}{\mathrm{d}T} = 0$

Table 3.2: Cases distinguished depending on the temperature increment when solidification takes part,($\Delta T = T_{n+1} - T_n$), [10]

3.5.2 Thermal behavior defined by UMATHT

The user subroutine UMATHT is used to define the thermal constitutive behavior of the material as well as internal heat generation during the heat transfer process. It can be used to define custom thermal models, such as those for phase change materials or for materials with temperature-dependent thermal conductivity.

Listing 3.2: User subroutine UMATHT interface

```
SUBROUTINE UMATHT(U,DUDT,DUDG,FLUX,DFDT,DFDG,
     1 STATEV,TEMP,DTEMP,DTEMDX,TIME,DTIME,PREDEF,DPRED,
     2 CMNAME,NTGRD,NSTATV,PROPS,NPROPS,COORDS,PNEWDT,
     3 NOEL,NPT,LAYER,KSPT,KSTEP,KINC)
C
      INCLUDE 'ABA_PARAM.INC'
C
      CHARACTER*80 CMNAME
      DIMENSION DUDG(NTGRD),FLUX(NTGRD),DFDT(NTGRD),
     1 DFDG(NTGRD,NTGRD),STATEV(NSTATV),DTEMDX(NTGRD),
     2 TIME(2),PREDEF(1),DPRED(1),PROPS(NPROPS),COORDS(3)


      user coding to define U,DUDT,DUDG,FLUX,DFDT,DFDG,
      and possibly update STATEV, PNEWDT


      RETURN
      END
```

In listing 3.2, U represents the internal thermal energy per unit mass at the end of an increment and FLUX(NTGRD) represents the heat flux vector also at the end of the increment. NTGRD is the number of spatial gradients of temperature, thus NTGRD=3 $(\frac{\partial T}{\partial x}, \frac{\partial T}{\partial y}, \frac{\partial T}{\partial z})$ for 3 dimensional heat flow. DUDT and DFDT represent the variation of internal thermal energy and the variaton of the heat flux vector respectively, with respect to temperature. DUDG and DFDG represent the variation of internal thermal energy and the variaton of the heat flux vector respectively, with respect to the spatial gradients of temperature. In order to model the thermal behavior of the material, it is necessary to define these quantities, since they are terms in the governing equation Eq.(2.30).
In this work, the thermal conductivity $k(T)$ and specific heat $c(T)$ are dependent on temperature, and a user subroutine is developed to calculate them through linear interpolation. Then they are called in UMATHT and if the element is active they are used to determine FLUX(NTGRD) based on Eq.(2.3) and U based on Eq(2.13) as seen in listing 3.3.

Listing 3.3: Internal energy U and heat flux vector FLUX(NTGRD),

Where SPECHT= $c(T) = \frac{\partial U(T)}{\partial T}$ and COND= $k(t)$

```
      DUDT = SPECHT
      DU = DUDT*DTEMP
      U = U+DU
C
      DO I=1, NTGRD
         FLUX(I) = -COND*DTEMDX(I)
         DFDG(I,I) = -COND
      END DO
```

All constraints and conditions that was developed in sections 3.3 and 3.4 for element activation and free surfaces calculation are implemented in UMATHT. The results are recorded in an array in binary form:

- 0 → inactive element, 1 → active element
- 0 → no boundary conditions at face N, 1 → boundary conditions at face N, for N=1,2,4,5,6 (face 3 is never a free surface in this model)

Then the results are saved in STATEV(NSTATV) which is an array containing the solution-dependent state variables. The results are also used in DFLUX during the boundary conditions application.

3.5.3 Boundary conditions at the substrate

The elements of the substrate are active from the start of the analysis. They are exposed to both convective and radiant boundary conditions. These conditions are modeled using the *FILM and *RADIATE keywords in ABAQUS software.

- FILM is used to define film boundary conditions, which represent a thin fluid layer that provides cooling to a model. It can be used to model convective boundary conditions.
- RADIATE is used to define radiant boundary conditions in heat transfer analyses, which are used to model the exchange of heat between surfaces due to radiation.

Chapter 4

3D simulation of Additive Manufacturing process and Results

4.1 Description of the Model Structure

A simulation of the additive manufacturing process with a moving heat source, in this case a laser beam, in three dimensions was carried out using the finite element formulation from chapter 3 to determine the thermal history of the process and calculate the temperature distribution. The scanning path of the laser beam's center, is described in detail in Section 3.1. As the beam moves, metal powder is fed into its path, melted by the heat source, and incorporated to the partially built component, while solidifying in the process.
The simulation model consists of a ($15\,mm \times 15\,mm \times 15\,mm$) substrate, upon which the metal deposition starts and a ($9\,mm \times 9\,mm \times 9\,mm$) cube is constructed through additive manufacturing. The processed part is built in 9 sequential layers of $1\,mm$ height each and every layer is built by 9 consecutive rows of material deposited of $1\,mm$ width each. Each row is generated by a single straight laser scan. For the finite element analysis, the substrate and the processed part are modeled with elements of the same type and dimensions of $1\,mm \times 1\,mm \times 1\,mm$. The DC3D8 element type was utilized during the thermal analysis, which is a 3D cubic element with 8 nodes and 8 integration points specifically designed for thermal analyses. The substrate consists of 3375 elements and 4096 nodes while the processed part consists of 729 elements and 1000 nodes. The model as a whole contains 4104 elements and 5096 nodes (with 100 of those nodes being shared).

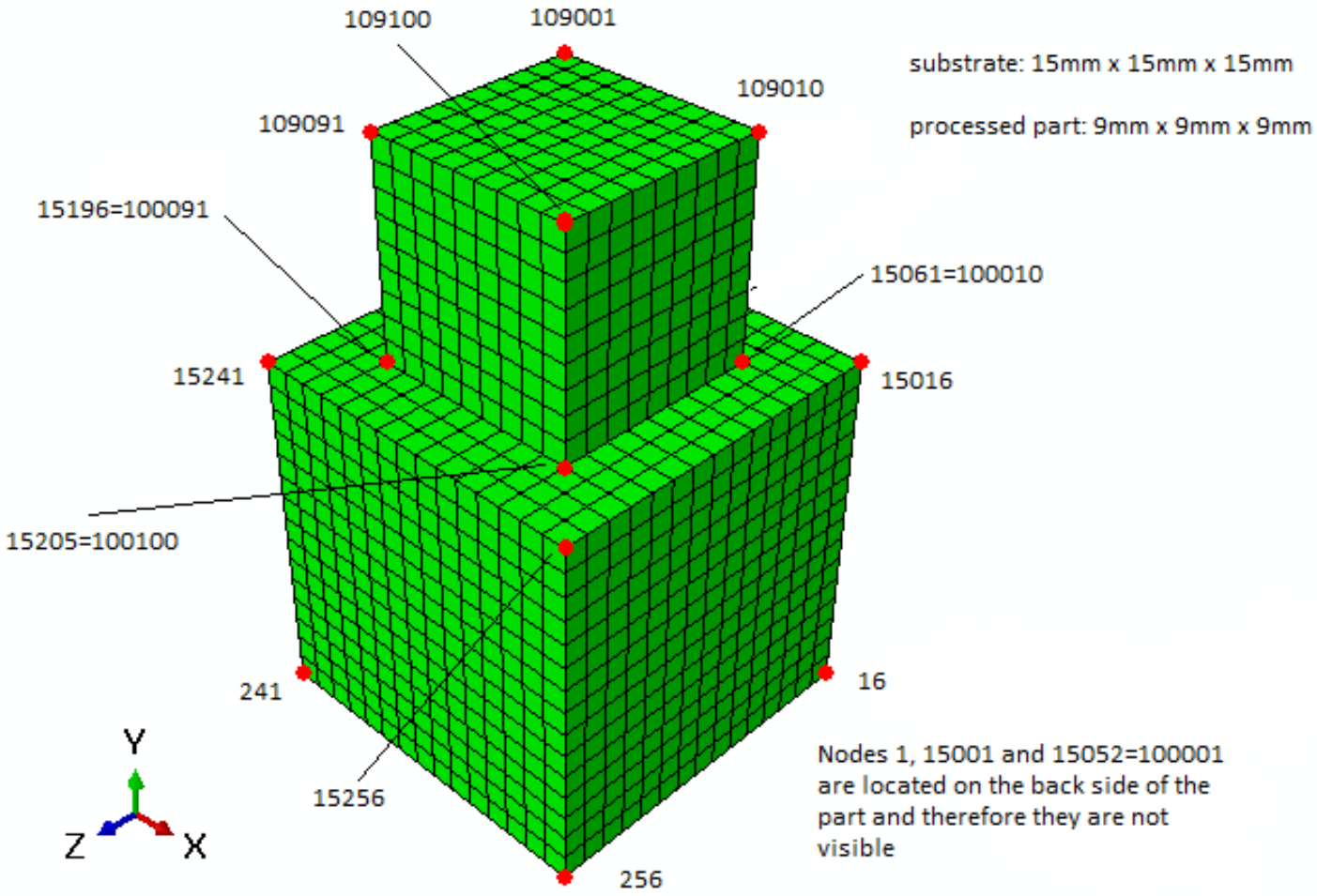

Figure 4.1: Model of the substrate and processed part used in the simulation

The material that is used in the simulation is an AISI 316L stainless steel. The thermal conductivity $k(T)$ and specific heat $c(T)$ are treated as temperature dependent in this study and their temperature-related values are shown in Table 4.1. The other properties of the material are quoted afterwards:

- Density $\rho = 8030\,\frac{kg}{m^3}$
- Heat transfer coefficient $h = 30\,\frac{W}{m^2\,K}$
- Emissivity $\epsilon = 0.5$
- Latent heat of fusion $U_{latent} = 330\,\frac{kJ}{kg}$
- Solidus temperature $T_S = 1400\,^\circ C$
- Liquidus temperature $T_L = 1459\,^\circ C$

It is worth noting that the heat transfer coefficient is set to $H = 630\,\frac{W}{m^2\,K}$, which is 21 times higher than $30\,\frac{W}{m^2\,K}$, and represents the localized forced convection within the heating zone. The heating zone is defined as a sphere with a 5mm radius centered around the moving heat source and was analyzed in Section 3.5.1.

The moving laser beam is modeled as an ellipsoidal volumetric heat source, as described in Eq.(3.1). The laser has a power of $P = 195\,W$ and a speed of $v = 20\,\frac{mm}{s}$. The semi-axes of the double ellipsoidal volumetric heat source have lengths of $(a, b, c) = (1mm, 1mm, 1mm)$. The time period during which the laser is inactive between consecutive rows within the same layer is set to $t^{idle}_{row} = 1\,s$, while the time period between the end of one layer and the start of the next, during which the laser remains inactive, is set to $t^{idle}_{layer} = 1.5\,s$. The additive manufacturing process starts at the point $(x^0_L, y^0_L, z^0_L,) = (3mm, 15mm, 3mm)$ of the substrate, where the laser is initially located, and its scanning path is described in detail in Section 3.1. In accordance with this model:

- $t_{row} = \frac{9\,mm}{20\,\frac{mm}{s}} = 0.45\,s$, represents the time needed to scan a single row along the x-axis.
- $t_{layer} = 9 \times t_{row} + 8 \times t^{idle}_{row} + t^{idle}_{layer} = 9 \times 0.45 + 8 \times 1 + 1.5 = 13.55\,s$, represents the time period from the start of one layer until the start of the following.
- $t_{process} = t_{layer} \times 9 - t^{idle}_{layer} = 13.55 \times 9 - 1.5 = 120.45\,s$, represents the duration of the process (until the laser finally stops).

Based on the position of the laser beam, when it is active, during the process the time period can be determined as:

$$t = (layer - 1) \times t_{layer} + (row - 1) \times (t_{row} + t^{idle}_{row}) + \frac{x}{20}$$

Lastly, the initial temperature of the substrate is set to $T_0 = 27\,^\circ C$ and the temperature of the surroundings is also $T_{surr} = 27\,^\circ C$.

Temperature T $[K]$	**Thermalconductivity** k $[\frac{W}{m\,K}]$	**Specific heat** c $[\frac{J}{kg\,K}]$
300	13.96	497.3066898
400	15.53	512.1102141
500	17.1	526.2479141
600	18.68	540.1130915
700	20.25	553.2918052
800	21.82	566.3414045
900	23.39	579.2475503
1000	24.96	592.096416
1100	26.53	604.9793395
1200	28.1	617.9957937
1300	29.67	631.1526351
1400	31.25	644.6809797
1500	32.82	658.3004952
1600	34.39	672.065387
1700	35.96	686.2039546
1701	17.98	769.0890406
1800	18.31	770.2831315
1900	18.64	770.9119574
2000	18.97	771.2212991
2100	19.3	771.2894359
2200	19.62	770.8003637
2300	19.95	770.6216031
2400	20.28	770.2370453
2500	20.61	770.1037393
2600	20.94	769.9174045
2700	21.26	769.574385
2800	21.59	769.8715172
2900	21.92	770.5081451
3000	22.25	771.3928407

Table 4.1: Thermal conductivity and specific heat for AISI 316L [26]

4.2 Results and discussion

This section is focused on the presentation of the results from the thermal analysis performed on the 3D additive manufacturing process, using the model structure and conditions outlined in section 4.1. The objective is to obtain the temperature distribution and thermal history generated during the process, which is crucial in assessing the resulting microstructure and determining the mechanical stresses and strains.

Firstly the accuracy of the model is validated, including the precise positioning of the laser beam, proper activation of elements, and correct application of boundary conditions on the free surfaces.
Figure 4.2 depicts the activation of 3 elements. Two of them (element 101073 in fig.4.2a and element 105081 in 4.2b) are part of the manufactured product while the third (element 12075 in fig.4.2c) belongs to the substrate, and we can observe that it is active from the beginning of the process as expected. Element 101073 is located in the second layer and in the last (ninth) row. It is the first element of its row and according to the process conditions described in section 4.1 it can be calculated that it is activated at $13.55 + 8 \times (0.45 + 1) = 25.15\,\text{sec}$. Element 105081 is the last element of the sixth layer and similarly it is activated at $13.55 \times 5 + 8 \times 1.45 + (8 - 1)/20 = 79.7\,\text{sec}$. The perfect match between these two timestamps and Figures 4.2a and 4.2b confirms the accuracy of the element activation model.

Figures 4.4 and 4.5 present a visual representation of the active elements in the model at different stages of the additive manufacturing process. To provide a clear view of the layer being formed at each time frame, a y-cut of the part is also shown.

In Figure 4.6, the elements of the processed part that have free surfaces and thus are exposed to boundary conditions at time t=88.6 seconds, are depicted. The red colour denotes that boundary conditions are applied to the element at the corresponding face. The last element to be activated at this time is situated in the second position of the sixth row in the seventh layer and elements with exposed free surfaces are identified in accordance with that. The elements that are exposed to convection and radiation are clearly and accurately shown in Figure 4.6, demonstrating that the model effectively determines the free surfaces.

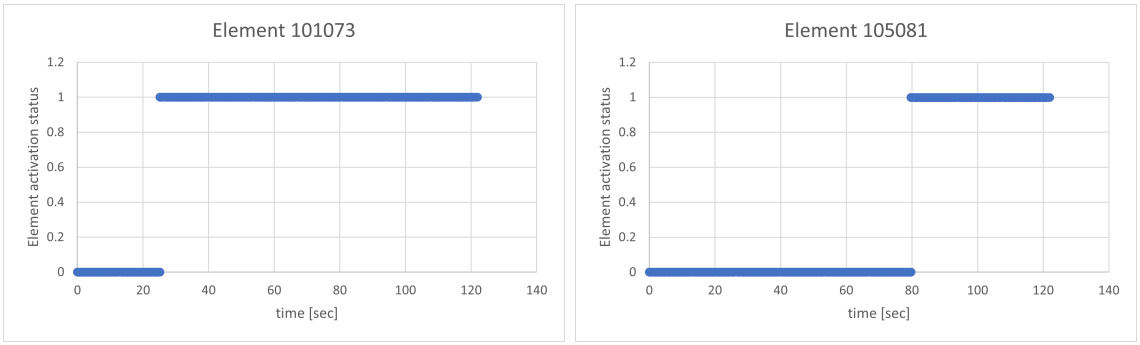

(a) Activated at $t = 25.15$ sec.

(b) Activated at $t = 79.7$ sec.

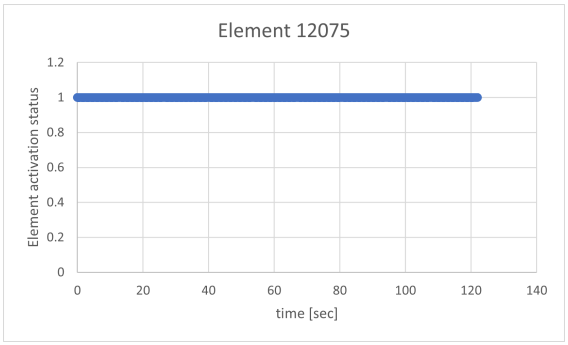

(c) Active from the start.

Figure 4.2: Element activation.

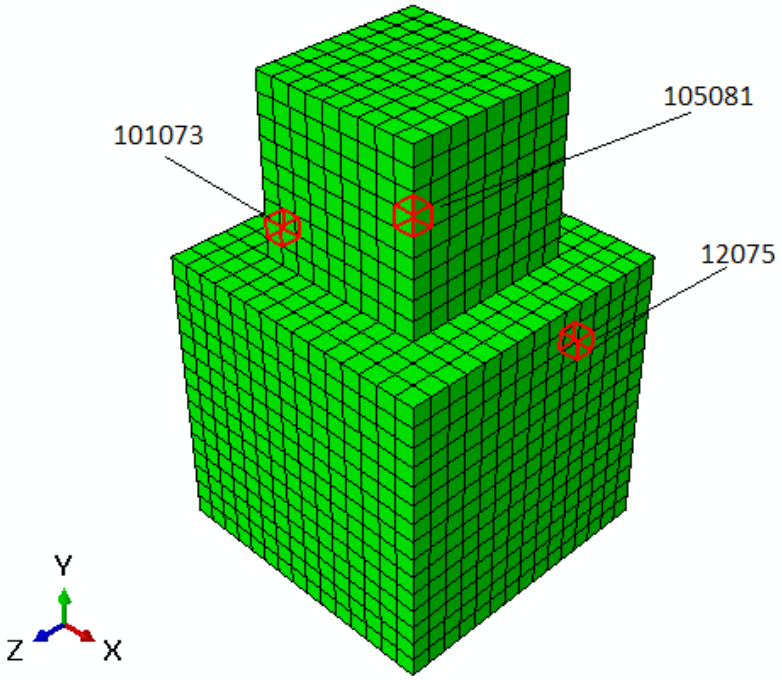

Figure 4.3: Location of elements 101073, 105081 and 12075

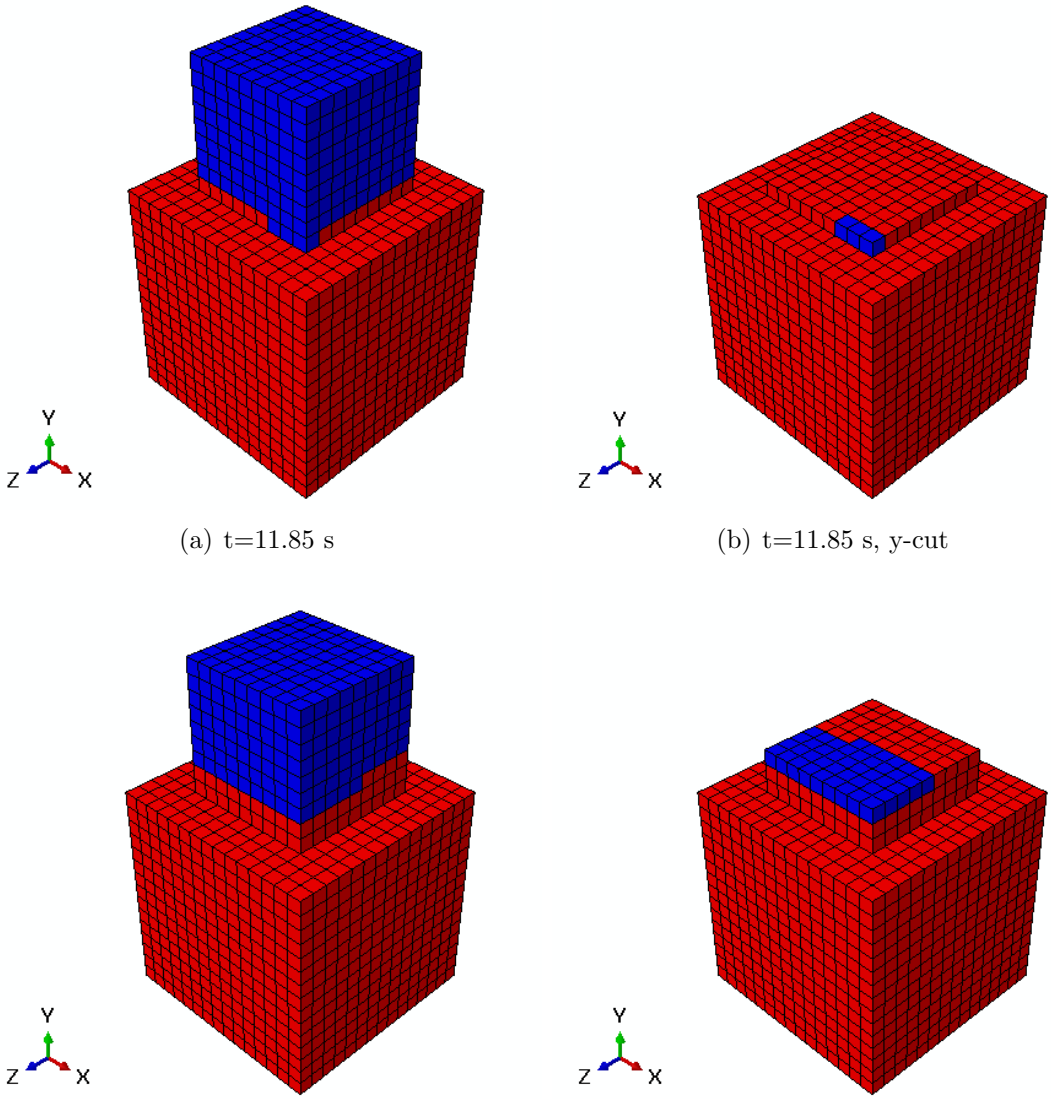

(a) t=11.85 s

(b) t=11.85 s, y-cut

(c) t=33 s

(d) t=33 s, y-cut

Figure 4.4: Activated elements visualization in different time frames (1)

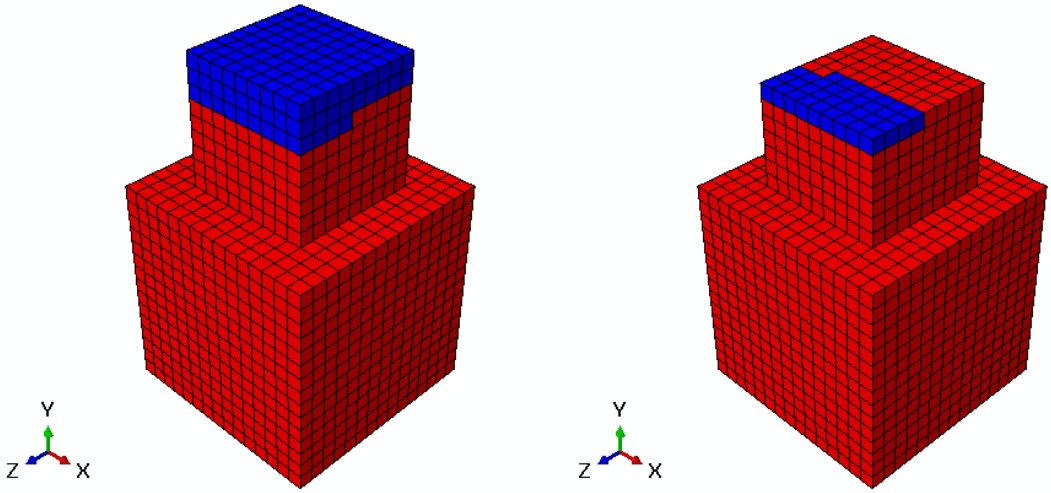

(a) t=88.6 s

(b) t=88.6 s, y-cut

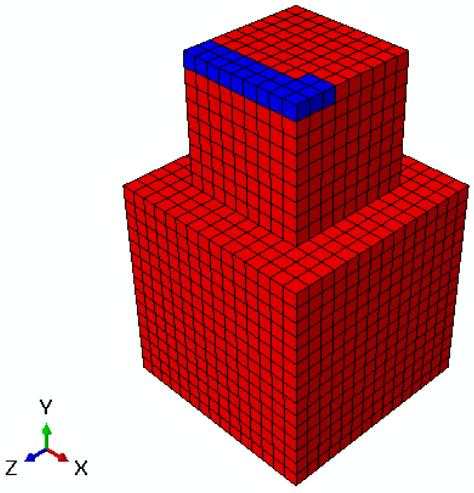

(c) t=117.35 s

Figure 4.5: Activated elements visualization in different time frames (2)

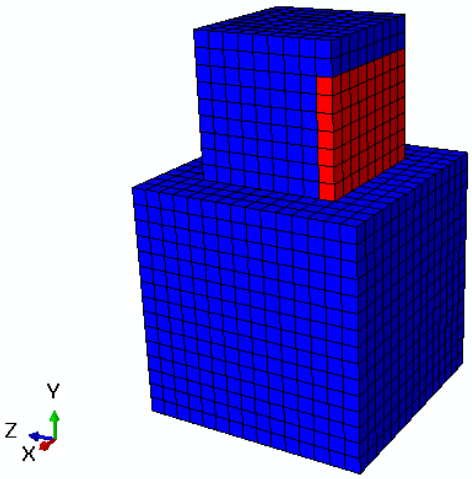

(a) Face 1

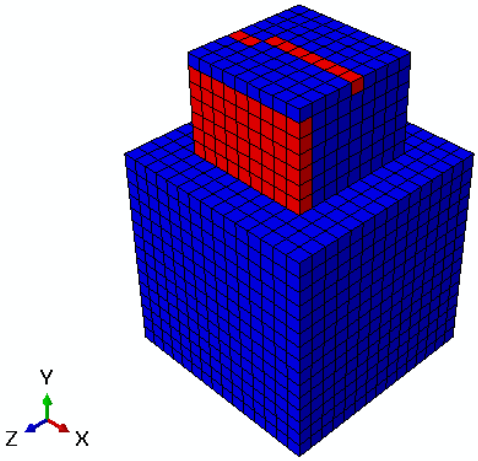

(b) Face 2

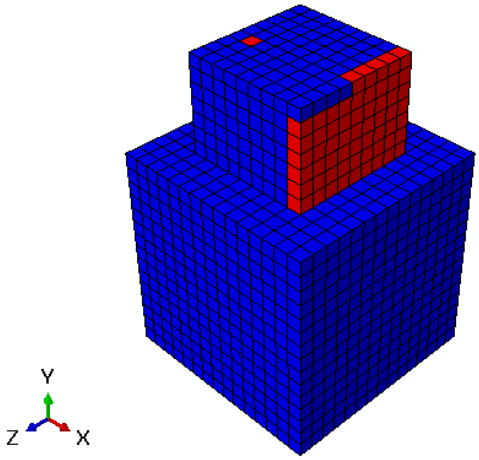

(c) Face 4

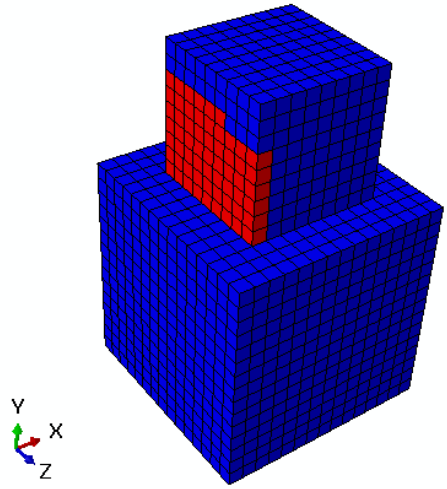

(d) Face 6

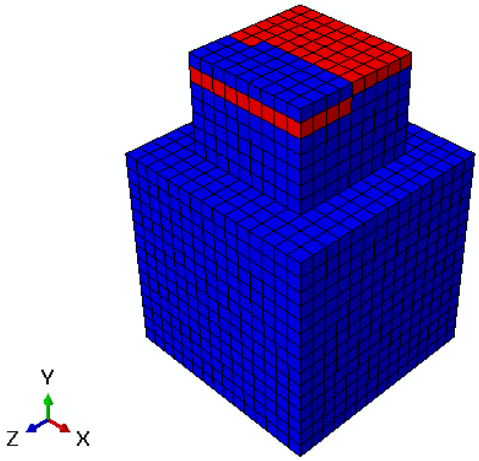

(e) Face 5a

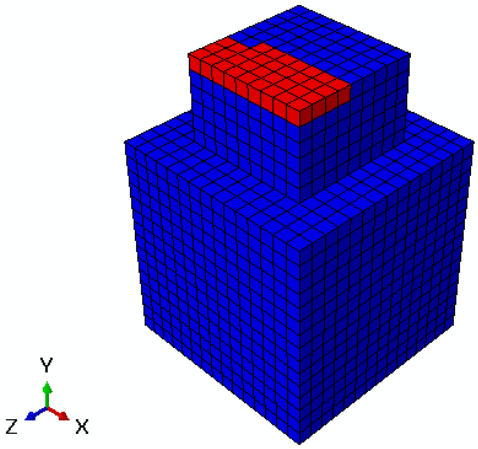

(f) Face 5b

Figure 4.6: Visualization of elements subjected to boundary conditions at t=88.6 s

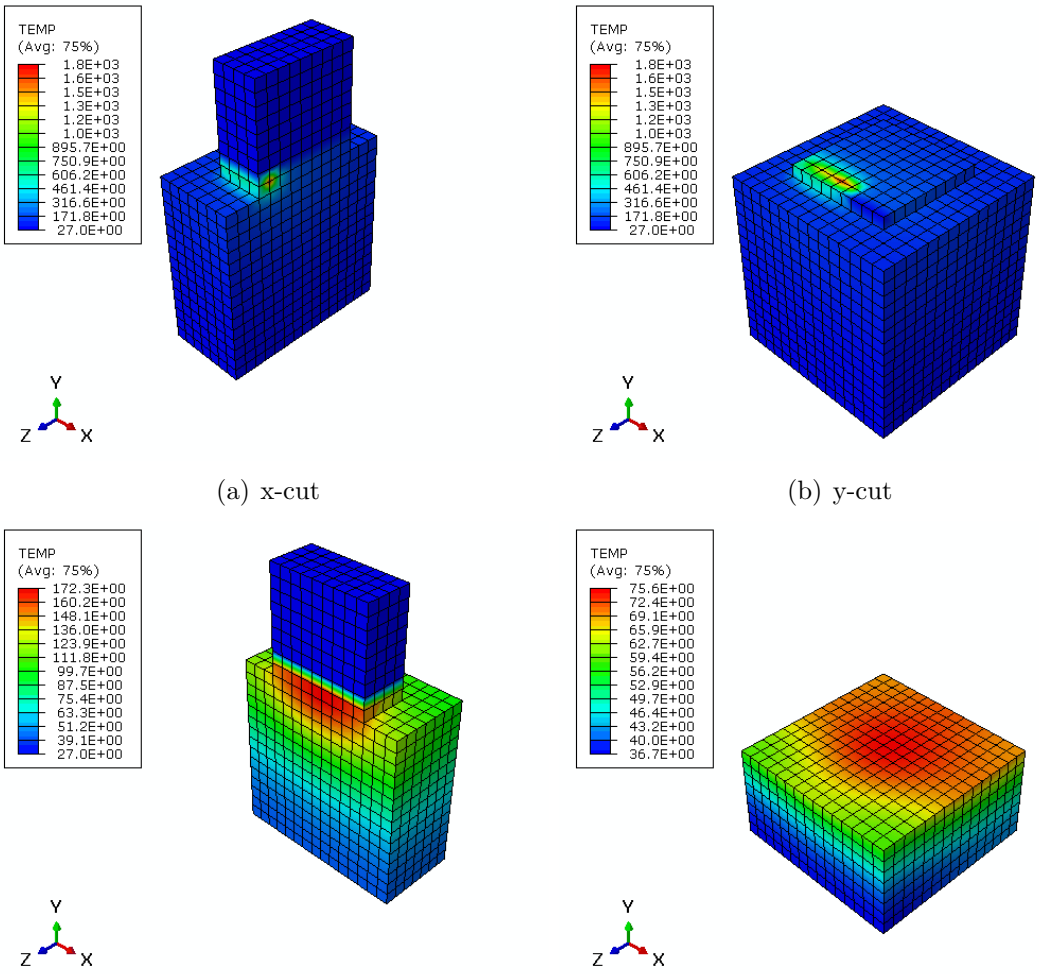

(a) x-cut

(b) y-cut

(c) z-cut

(d) substrate y-cut

Figure 4.7: Temperature field (^oC) at t=11.85 s, the laser is active.

Illustrated in Figures 4.7, 4.8, 4.9, 4.10, and 4.11 are the temperature distributions at various stages of the process. The figures show that when the laser is active, as depicted in fig.4.7, 4.9, and 4.10, temperatures reach significantly higher values compared to when the heat source is inactive (rapid decrease in temperature), as shown in fig.4.8 and 4.11, resulting in significant temperature fluctuations and changes during the process. In addition to the high temperature variations throughout the process, it is also noticeable that the temperatures around the center of the laser beam reach significantly higher levels, showing a concentrated distribution of heat in the molten pool. It can be seen that the maximum temperatures continue to rise as the process progresses, with the center of the laser reaching 1800 ^oC in fig.4.7 and 2200 ^oC in fig.4.10. As the process progresses, the temperature in the remote zones of the substrate, as observed in the y-cut, gradually increases.

The temperature field is depicted in cross-sectional views in all directions and at the substrate to clearly show the temperature distribution in all figures.

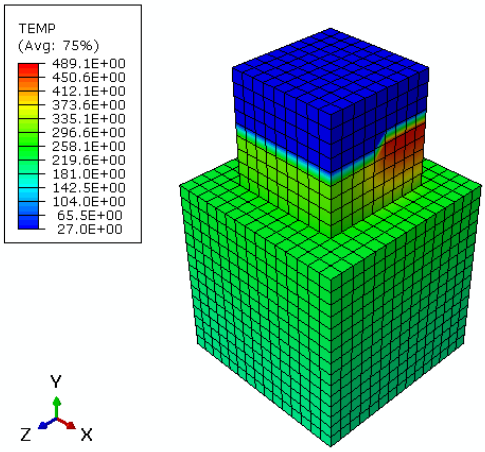

(a) Entire part

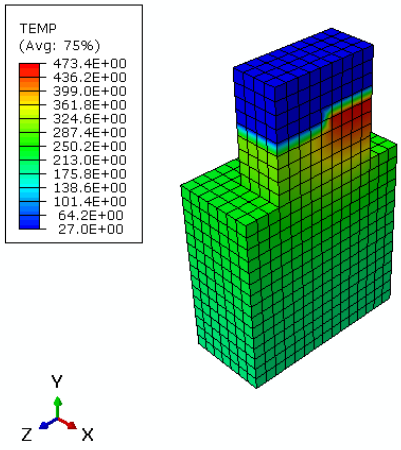

(b) x-cut

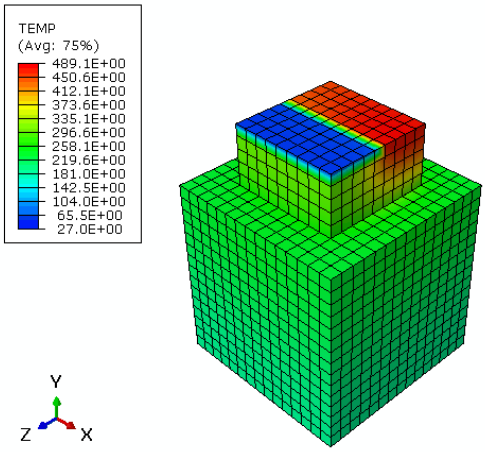

(c) y-cut

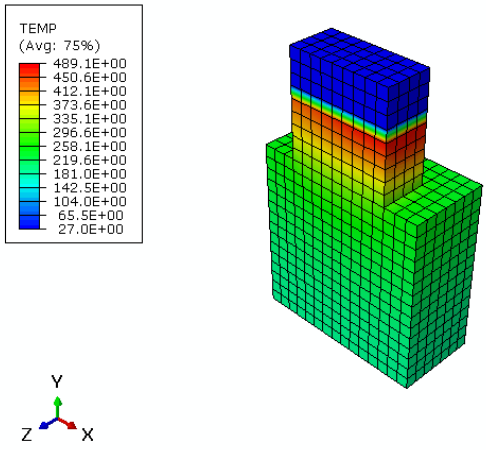

(d) z-cut

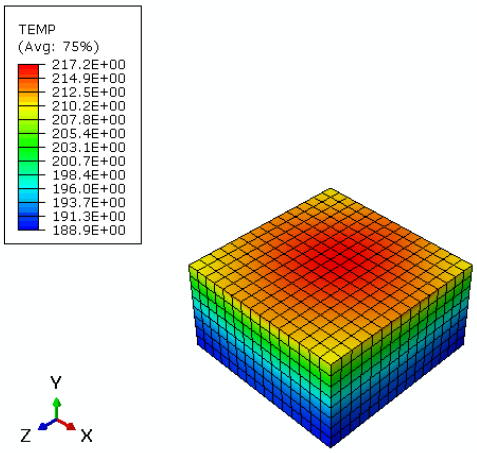

(e) substrate y-cut

Figure 4.8: Temperature field (^oC) at t=59.75 s, the laser is idle.

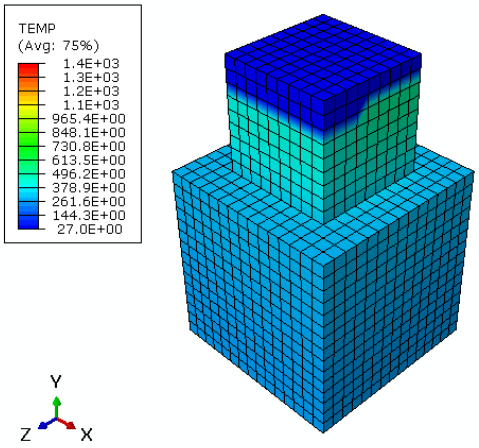

(a) Entire part

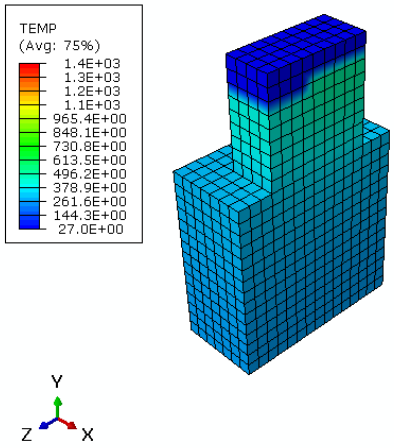

(b) x-cut

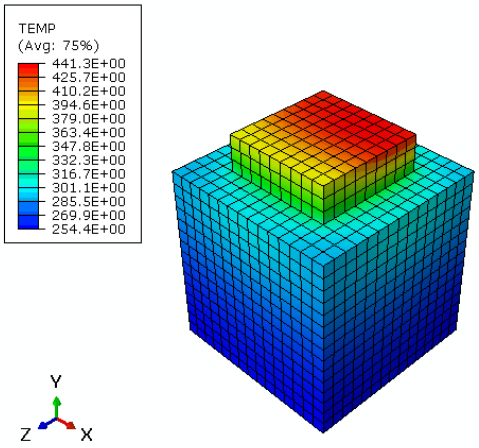

(c) y-cut

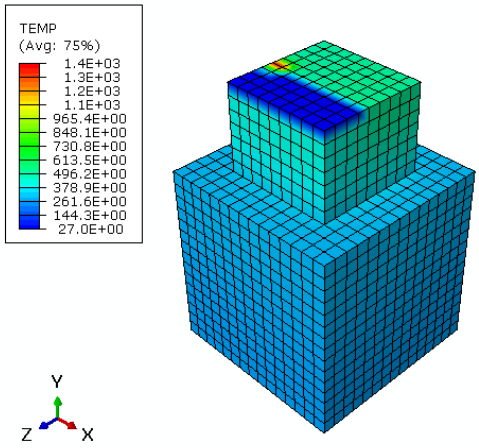

(d) y-cut at the processed layer

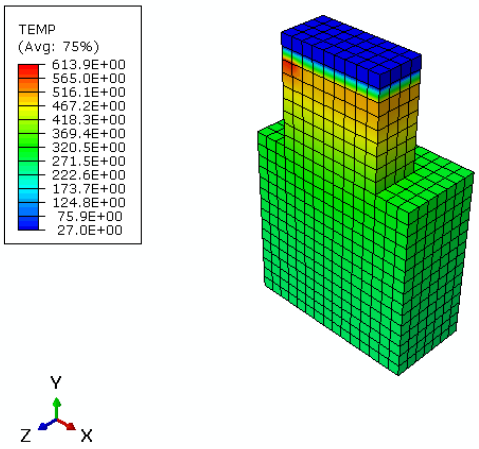

(e) z-cut

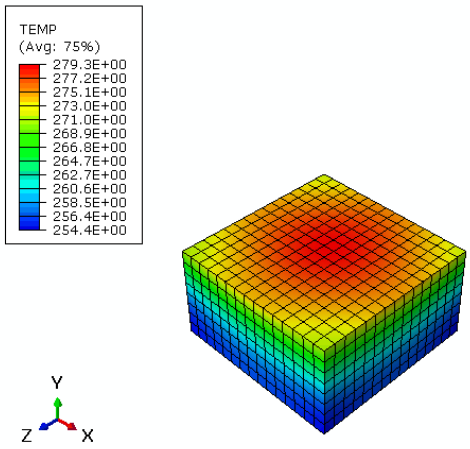

(f) substrate y-cut

Figure 4.9: Temperature field (^oC) at t=88.6 s, the laser is active.

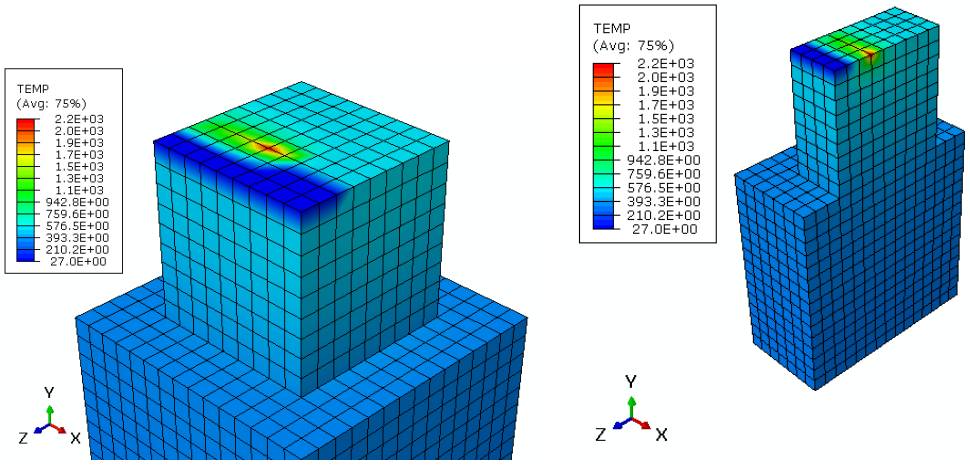

(a) Entire part

(b) x-cut

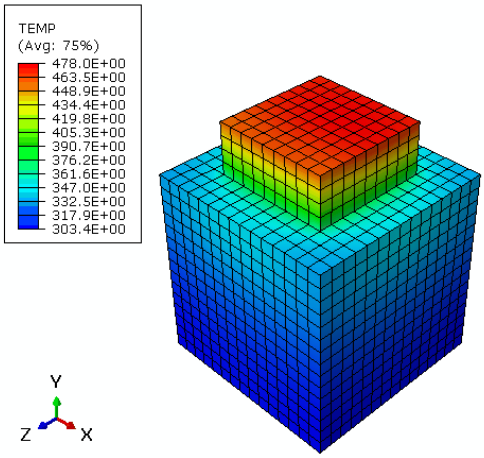

(c) y-cut

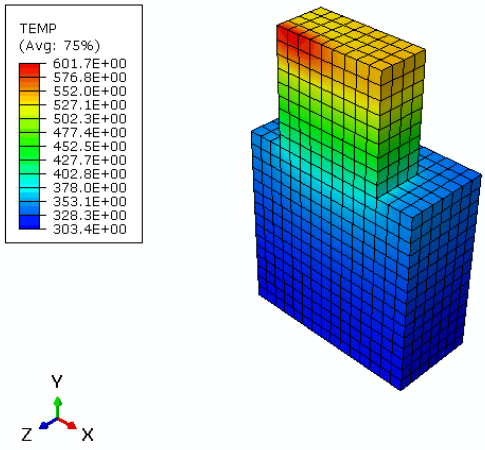

(d) z-cut

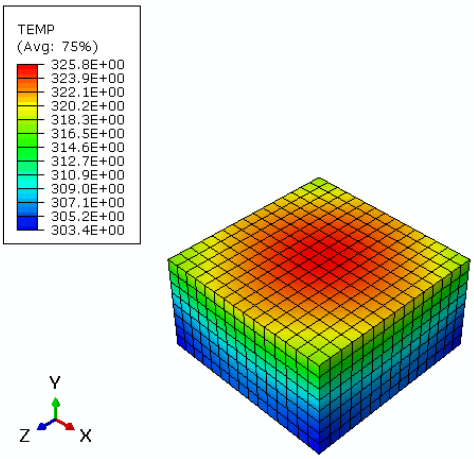

(e) substrate y-cut

Figure 4.10: Temperature field (^oC) at t=117.35 s, the laser is active.

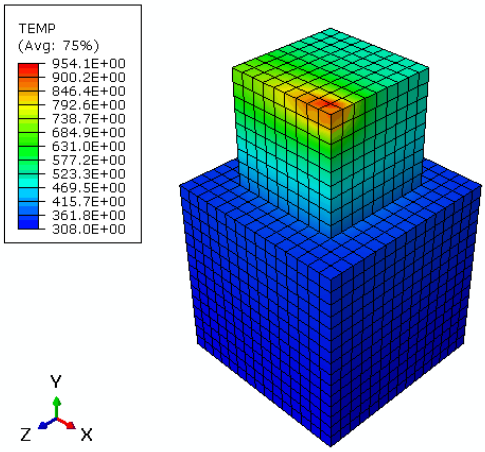

(a) Entire part

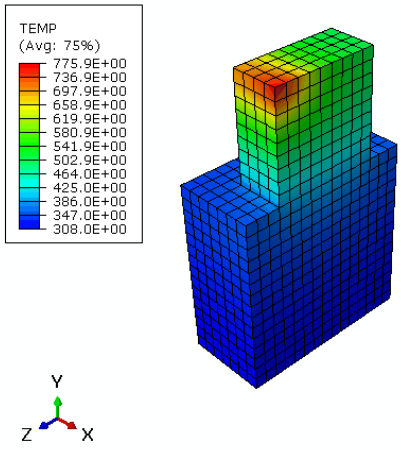

(b) x-cut

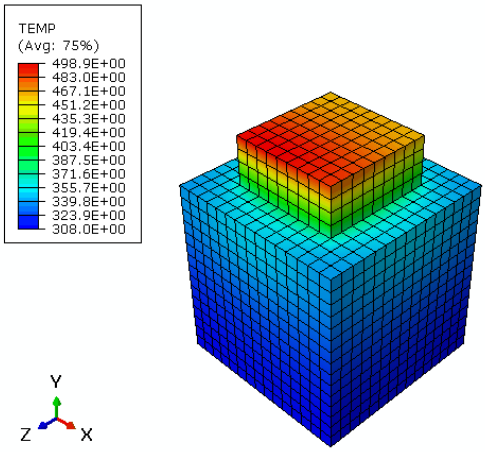

(c) y-cut

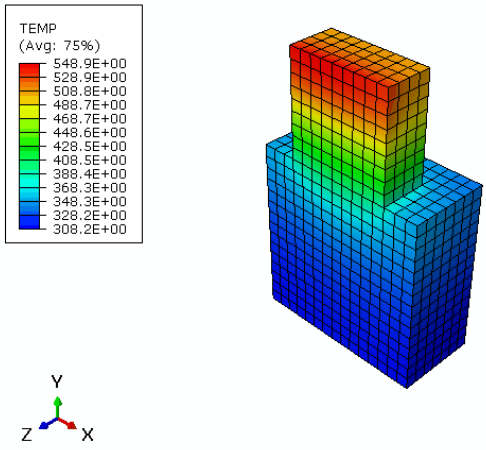

(d) z-cut

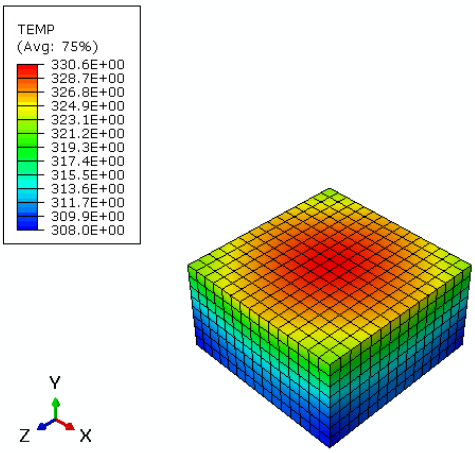

(e) substrate y-cut

Figure 4.11: Temperature field (^oC) at t=120.7 s, the laser is idle.

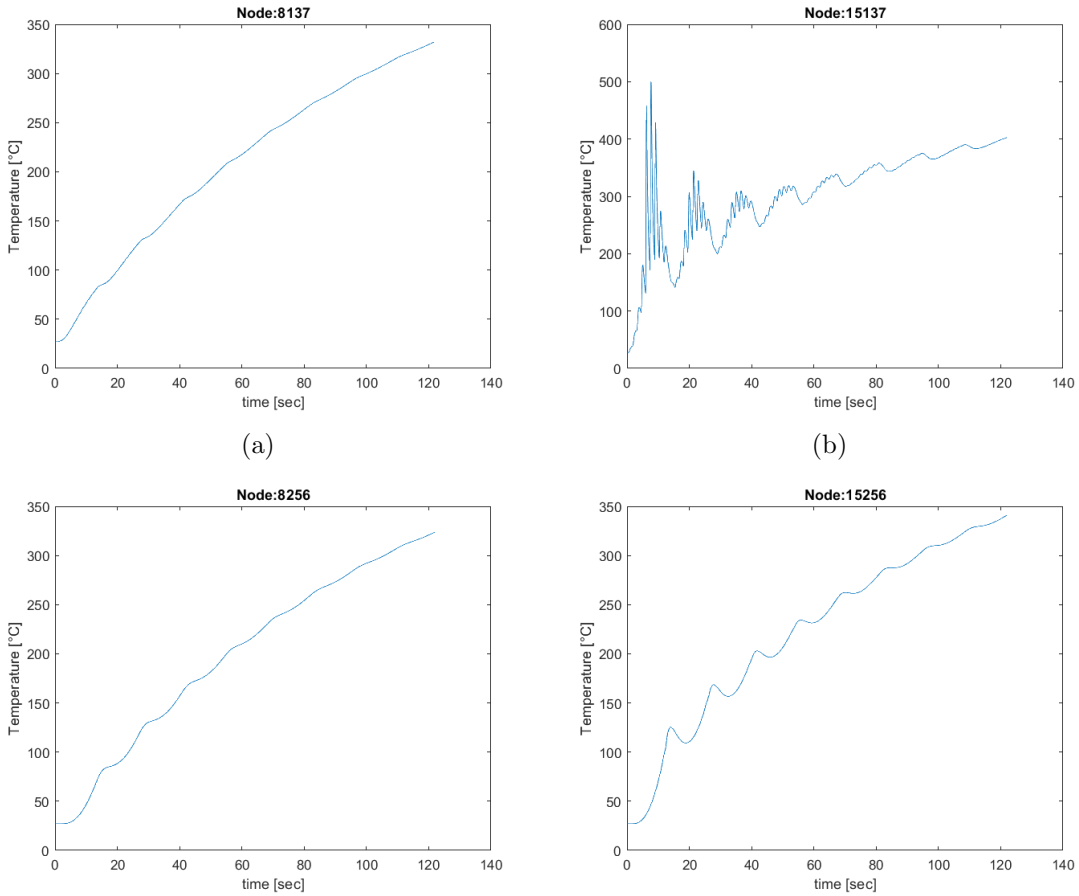

Figure 4.12: Temperature history of the substrate over time

The temperature history of four substrate nodes is depicted in Figure 4.12. Nodes 8137 (fig.4.12a) and 8256 (fig.4.12c) are located in the center of the substrate along the y-axis, with 8137 located within the substrate and 8256 on the boundary. Nodes 15137 (fig.4.12b) and 15256 (fig.4.12d) are situated in comparable positions to 8137 and 8256 regarding the x-z plane, but on the upper boundary of the substrate. We can observe that the temperature steadily rises over time in figures 4.12a, 4.12c and 4.12d, however in fig.4.12b the temperature experiences fluctuations due to the node 15137 being directly under the region where the laser was active.

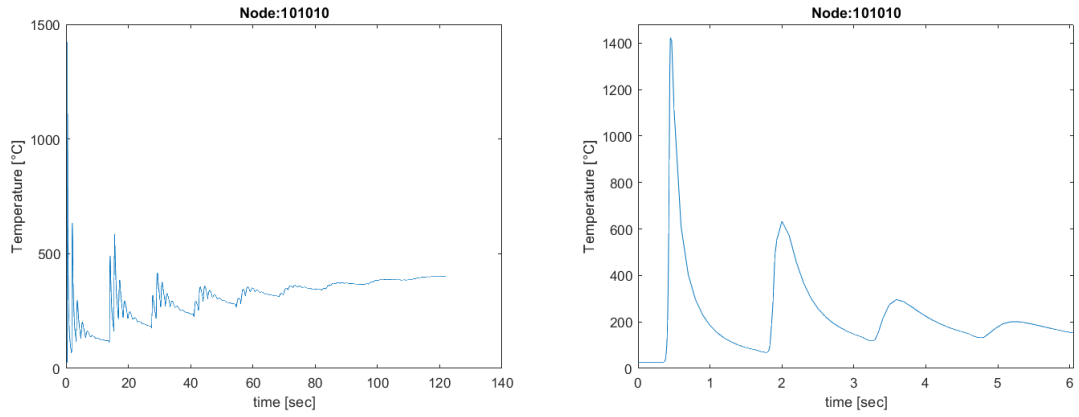

(a) (b) zoom in

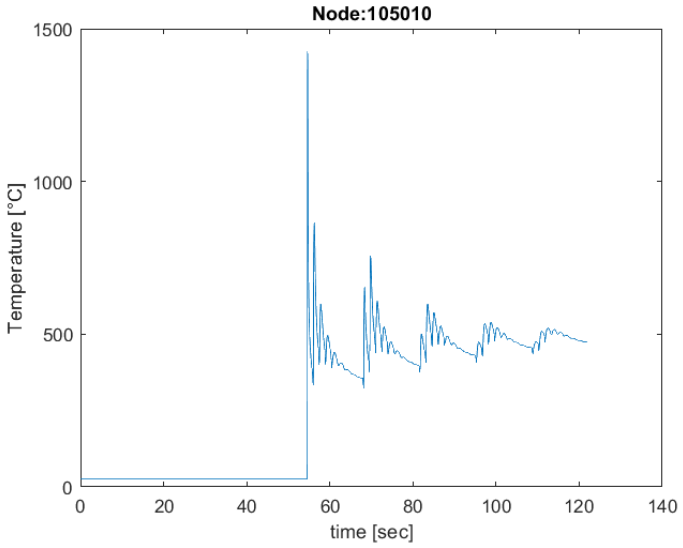

(c)

Figure 4.13: Temperature history on the boundary of the processed part over time

The temperature history of two boundary nodes of the processed part is shown in Figure 4.13. A rapid temperature rise of both nodes (node 101010 in fig.4.13a and node 105010 in fig.4.13c) is observed as soon as the element they belong to is activated. A close-up view of the activation of node 101010 can be seen in fig.4.13b, where the clear initial temperature spike is a result of the laser passing over the node. The two figures present similar patterns immediately after activation, as a consequence of the repeated heating-cooling cycle until the process is over.

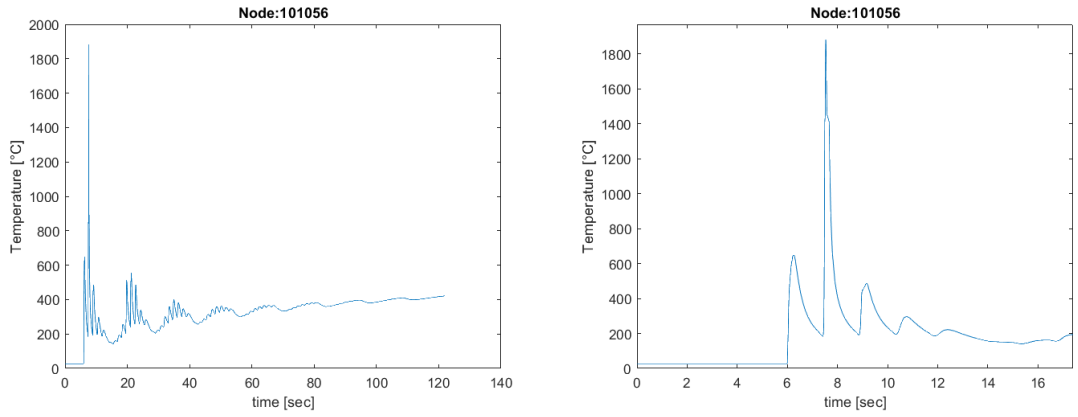

(a) (b) zoom in

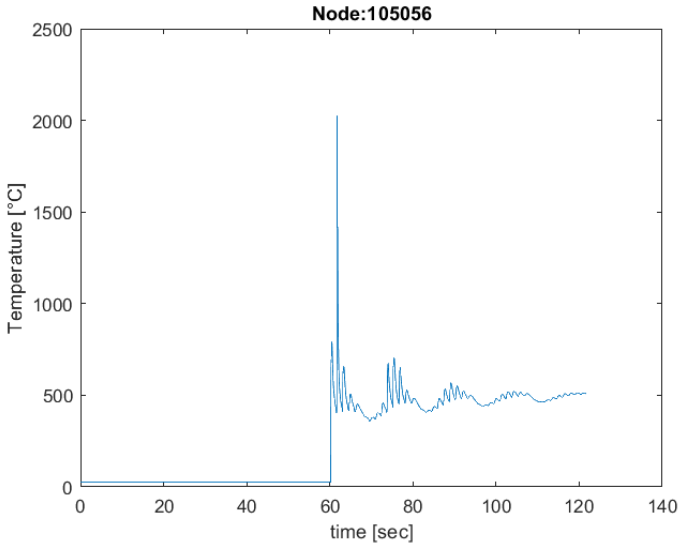

(c)

Figure 4.14: Temperature history in the middle of the processed part over time

In Figure 4.14, the nodes for which temperature history is displayed in figures 4.14a (node 101056) and 4.14c (node 105056) are situated in the center of the processing part. The temperature histories look similar to those shown in Figure 4.13 and follow a similar cyclic pattern. However, there are two main differences. Firstly higher temperatures are observed for nodes in the middle compared to those at the boundary. Moreover, as seen in fig.4.14b, the peak nodal temperature does not happen during the element's activation. This is because the initial temperature spike occurs when the laser passes from the preceding node during activation. The subsequent high temperature spike occurs as the laser passes through the node, and the third, lower temperature spike occurs when the laser moves on to the next node as it scans the layer.

Overall the temperature history of nodes on the processed part presents a cyclic upward

pattern, due to cooling and heating cycles and rapid spikes when the laser passes near them. Additionally, the temperature is higher in the center than at the boundaries and the maximum temperatures are bigger in upper layers than in lower ones. Lastly nodes of the substrate that are closer to the heat source experience higher temperature fluctuations while the temperature of nodes further away from the heat source rises more steadily.

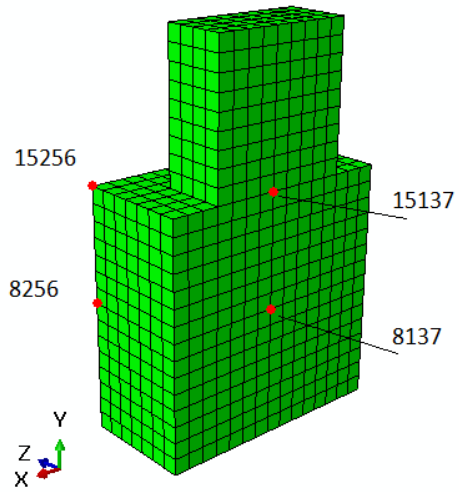

(a)

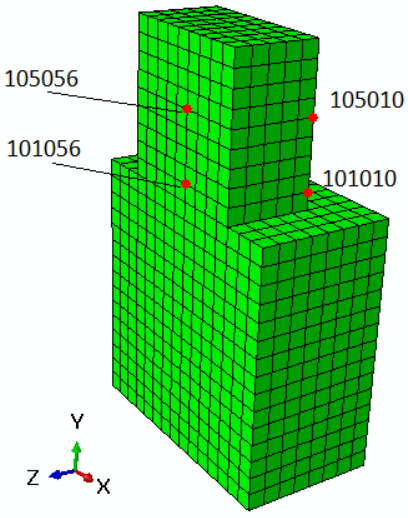

(b)

Figure 4.15: (a) Location of nodes 8137, 8256, 15137 and 15256 on the substrate, (b) Location of nodes 101010, 101056, 105010 and 105056 on the built part.

Chapter 5

Conclusion

This diploma thesis presents a three-dimensional model aimed at investigating the thermal behavior and calculating the temperature field of laser-based additive manufacturing processes for metallic parts. The theoretical formulation of thermal analysis was implemented using the finite element software ABAQUS, and the model was applied for an AISI 316L stainless steel.
According to the results of the simulation, it is evident that the model accurately simulates the laser-based additive manufacturing process. More specifically, the element activation and material deposition were simulated successfully based on the scanning path of the laser and process parameters. Inactive elements did not affect the analysis due to the effectiveness of the modified quiet element method. The location of the evolving interface between active and inactive elements was calculated correctly and boundary conditions were accurately applied on each free surface. Furthermore, the temperature history generated by the model seems to be accurate for both the substrate and the built part.
The purpose of this work was to develop a model that simulates the laser-based additive manufacturing processes and extracts the temperature field which can be used to study the mechanical and microstructural behavior in order to eventually improve the quality of the product and efficiency of the process. The model can be easily modified, allowing for the adjustment of material and process parameters, in order to be used in various applications. Here are some recommendations for future work:

- Utilize the temperature field in the mechanical analysis to estimate the thermal stresses and strains.
- Develop a thermomechanical coupled model to reduce computational time.
- Modify the model to take into account the metal powder.
- Utilize the temperature history to evaluate the resulting microstructure.

Bibliography

[1] I. Gibson, D. Rosen, B. Stucker, 'Additive Manufacturing Technologies', second edition, (2015)

[2] A. Uriondo, M. Esperon-Miguez, S. Perinpanayagam, 'The present and future of additive manufacturing in the aerospace sector: A review of important aspects', Journal of Aerospace Engineering (2015)

[3] I. Yadroitsev, P. Krakhmalev, 'Selective laser melting of Ti6Al4V alloy for biomedical applications: Temperature monitoring and microstructural evolution', Journal of Alloys and Compounds (2015) 404-409

[4] B. Baufeld, O. Van der Biest, R. Gault, 'Additive manufacturing of Ti–6Al–4V components by shaped metal deposition: Microstructure and mechanical properties', Materials and Design (2010) S106–S111

[5] M. P. Sotiriou, J. S. Aristeidakis, M.I. T. Tzini, I. Papadioti, G. N. Haidemenopoulos, N. Aravas, 'Microstructural and Thermomechanical Simulation of the Additive Manufacturing Process in 316L Austenitic Stainless Steel', Mater. Proc. (2021), 3(1), 20

[6] N. Ahmed, I. Barsoum, G. Haidemenopoulos, R.K. Abu Al-Rub, 'Process parameter selection and optimization of laser powder bed fusion for 316L stainless steel: A review', Journal of Manufacturing Processes (2022) 415-434

[7] A. Vasinonta, J. L. Beuth, M. Griffith, 'Process Maps for Predicting Residual Stress and Melt Pool Size in the Laser-Based Fabrication of Thin-Walled Structures', J. Manuf. Sci. Eng. (2007) 101-109

[8] K. Saeidi, X. Gao, Y. Zhong, Z.J. Shen, 'Hardened austenite steel with columnar sub-grain structure formed by laser melting', Materials Science and Engineering A (2015) 221-229

[9] K. Dai, L. Shaw, 'Distortion minimization of laser-processed components through control of laser scanning patterns', Rapid Prototyping Journal (2002) 270-276

[10] L.A. Spyrou, N. Aravas 'Thermomechanical modeling of laser spot welded solar absorbers', Journal of Manufacturing Science and Engineering (2015)

[11] L.E. Lindgren, 'Computational Welding Mechanics. Thermomechanical and Microstructural Simulations', (2007)

[12] Van der Aa, E., 'Finite Element Modelling of Temperature Profiles, Distortions and Residual Stresses due to TIG Welding', (2002)

[13] L.E Lindgren, E. Hedblom, 'Modelling of addition of filler material in large deformation analysis of multipass welding', (2001)

[14] P. Michaleris, 'Modeling metal deposition in heat transfer analyses of additive manufacturing processes', Finite Elements in Analysis and Design (2014) 51-60

[15] L. Costa, R. Vilar, T. Reti, R. Colaço, A. M. Deus, I. Felde, 'Simulation Of Phase Transformations In Steel Parts Produced By Laser Powder Deposition', Materials Science Forum (2005) 473-474:315-320

[16] T. Zacharia, S. A. David, J. M. Vitek and T. Debroy, 'Weld Pool Development during GTA and Laser Beam Welding of Type 304 Stainless Steel, Part II—Experimental Correlation', (1989)

[17] J. Goldak, A. Chakravarti and M. Bibby, 'A New Finite Element Model for Welding Heat Sources', Metallurgical Transactions B (1984) 299–305

[18] J.C. Heigel, P. Michaleris, E.W. Reutzel, 'Thermo-mechanical model development and validation of directed energy deposition additive manufacturing of Ti–6Al–4V', Additive Manufacturing (2015) 9-19

[19] ABAQUS, Analysis User's Manual, Version 6.14, © Dassault Systémes, 2014.

[20] R. Ye, J. E. Smugeresky, B. Zheng, Y. Zhou, E. J. Lavernia, 'Numerical modeling of the thermal behavior during the LENS® process', Materials Science and Engineering A (2006) 47–53

[21] L. Costa, R. Vilar, T. Reti, A.M. Deus 'Rapid tooling by laser powder deposition: Process simulation using finite element analysis', Acta Materialia 53 (2005) 3987–3999

[22] J. Ding, P. Colegrove, J. Mehnen, S. Ganguly, P.M. Sequeira Almeida, F. Wang, S. Williams, 'Thermomechanical analysis of Wire and Arc Additive Layer Manufacturing process on large multi-layer parts', Computational Materials Science (2011) 3315-3322

[23] J. H. Lienhard iv and J. H. Liehnard v, 'A heat transfer textbook', fifth edition, (2020)

[24] Y. A. Cengel, 'Heat transfer; a practical approach', second edition, (2002)

[25] A. M. Malik, E. M. Qureshi, N. U. Dar and I. Khan, 'Analysis of circumferentially arc welded thin-walled cylinders to investigate the residual stress fields', Thin-Walled Structures (2008) 1391-1401

[26] C. S. Kim, 'Thermophysical properties of stainless steels', (1975)